THE JOURNAL OF COMPARATIVE NEUROLOGY 375:89–108 (1996)

# Distributed Representation of Vibrissa Movement in the Upper Layers of Somatosensory Cortex Revealed With Voltage-Sensitive Dyes

D. KLEINFELD AND K.R. DELANEY
Biological Computation Research Department, Bell Laboratories, Lucent Technologies, Murray Hill, New Jersey 07974 (D.K.); Department of Biosciences, Simon Fraser University, Burnaby, British Columbia, V5A 1S6 Canada (K.R.D.)

ABSTRACT

We have identified large-scale patterns of electrical activity in cortical circuits that occur in response to stimulation of peripheral receptors. Our focus was on primary (S1) vibrissal cortex of anesthetized rat, and we used optical techniques in conjunction with voltage-sensitive dyes to measure depolarization of the upper layers of cortex. Displacement of one vibrissa produced a field of activity that extends over very many cortical columns in S1. There are multiple, focal maxima within this field. A global maximum is located near the center of the field of activity, and, as determined electrically and histologically, this site maps to the cortical column appropriate for the deflected vibrissa. The amplitude of this component attains a steady-state value under continuous stimulation. Additional temporal characteristics are revealed by the response to a single displacement; the signal was triphasic and began with a prompt depolarization that was followed by a transient phase of inhibition and a final phase of long-lasting depolarization. The somatotopy of the other, satellite maxima in the field of activity were established through the reconstruction of the fields of activity produced by individual stimulation of other vibrissae. Local maxima for one vibrissa were seen to overlie the global maximum found for stimulation of nearest- and next-nearest-neighbor vibrissae. In contrast to the amplitude of the global maxima, the amplitude associated with the local maxima was not maintained with either continuous or infrequent but repetitive stimulation. Finally, the field of activity induced by alternate deflection of two neighboring vibrissae was suppressed in amplitude in comparison to the summed amplitudes of the signals elicited by deflection of each vibrissa alone. We suggest that these patterns of activity are a manifestation of the dynamic interaction among neighboring cortical columns. 

**Indexing terms: barrel cortex, electrical activity, functional imaging, lateral interactions, whiskers**

Primary sensory areas of mammalian neocortex integrate spike-coded information that arrives from sensory pathways and efferent cortical pathways. The latter pathways involve interactions with neighboring columns that generally respond to the same stimulus modality as well as interactions with distant cortical areas that subserve such functions as motor output or memory. A fundamental site of integration among these different sources of neuronal input is the upper layers of cortex. In particular, neurons in layers 2/3 and their dendrites receive input from sensory pathways via layer 4, from nearby columns via layers 2/3 and layer 5 "horizontal" connections, and from higher cortical areas via efferents to layer 1 (see, e.g., Lund, 1988). Furthermore, the upper layers of cortex encompass the dendrite fields from at least one subclass of neurons in layer 5 (Kim and Connors, 1993); thus, activity in layers 2/3 serves as a window to probe activation of an entire cortical column.

In this work we focus on the spatial distribution and slow temporal dynamics of activity in layers 2/3 of vibrissa primary and secondary sensory cortex in juvenile rat. There are several experimental advantages to this system. First, there is a one-to-one topography between vibrissa location on the mystacial pad and vibrissa representation in cortex (Fig. 1; Woolsey and van der Loos, 1970), so displacement of

Accepted June 12, 1996.

Address reprint requests to David Kleinfeld, Department of Physics 0319, University of California, 9500 Gilman Drive, La Jolla, CA 92093. E-mail: dk@physics.ucsd.edu

a single vibrissa leads to single-unit activity in layer 4 predominantly within one column (Welker, 1971). Second, the system develops early; i.e., juvenile animals exhibit mature whisking (Welker, 1964), essentially fully developed neuronal properties (McCormick and Prince, 1987), and refined intracortical connectivity (Nicolelis et al., 1991). This allows us to exploit postnatal day (P) 15–22 animals that have relatively optically clear cortices compared to adults.

Prior studies have shown that vibrissa-related activity is not restricted to a single column but spreads from layer 4 to the deeper and superficial layers of that column and neighboring columns (Armstrong-James and Fox, 1987; Welker et al., 1988). The nature of this spread has been the subject of anatomical and physiological studies. Intracortical tracing studies show that there are column-to-column horizontal connections in layers 2/3 and 5 (Bernardo et al., 1990a,b) that are largely confined to nearest-neighbor cortical columns but also extend sparsely to distant columns. A spread of activation between neighboring columns is also inferred from measurements of deoxyglucose uptake; stimulation of a single vibrissa led to heightened metabolic activity throughout the topographically appropriate as well as neighboring columns (Chmielowska et al., 1986; McCasland and Woolsey, 1988) and the nearby septal regions between neighbors (Kossut et al., 1988). Single-unit studies show that the horizontal spread among neighboring columns extends at least to next-nearest neighbors (Armstrong-James et al., 1991) and may involve corticothalamic feedback pathways (Diamond et al., 1992a,b) as well as intracortical connections. Finally, optical studies of preparations stained with voltage-sensitive dyes show that stimulation of a single vibrissa leads to a depolarization that extends over ~ 1,500 μm (Orbach et al., 1984); this distance is sufficient to encompass many neighbors. In toto, these prior studies support the notion that large-scale electrical activity in layers 2/3 is a manifestation of column-to-column interactions.

Herein we further explore the space and time dependence of the spread of electrical activity in the upper layers of barrel cortex. Our study is biased toward questions that can be addressed through the use of optical imaging in conjunction with preparations stained with voltage-sensitive dyes. These measurements are sensitive to changes in the membrane potential of neurons and largely report spatially averaged changes in the depolarization of dendritic fields; as such, these measurements provide data that are complementary to data based on single-unit and deoxyglucose uptake measurement. Previous application of this technique to primary vibrissa cortex (Orbach et al., 1984; London et al., 1989) and primary visual cortex (Orbach et al., 1984; Orbach and Van Essen, 1993; Grinvald et al., 1994) yielded information on the spatial extend and rate of lateral spread of activity and, recently, on some aspects of space-time coherence of activity (Arieli et al., 1995). The present study advances this optical technique to delineate further the spatial structure of stimulus-evoked activation of the upper layers of vibrissae cortex. Finally, selected aspects of our measurements are compared to measurements obtained with conventional electrophysiological and histological techniques.

We asked the following questions. 1) In response to motion of a single vibrissa, is the spatial structure of the activation in the upper layers of cortex uniform, or does it exhibit systematic variations? 2) How do the locations of responses for different vibrissae compare with the known topography of vibrissal representation in cortex? 3) What is the time dependence of the (subthreshold) activity in the upper layers, particularly in comparison with past single-

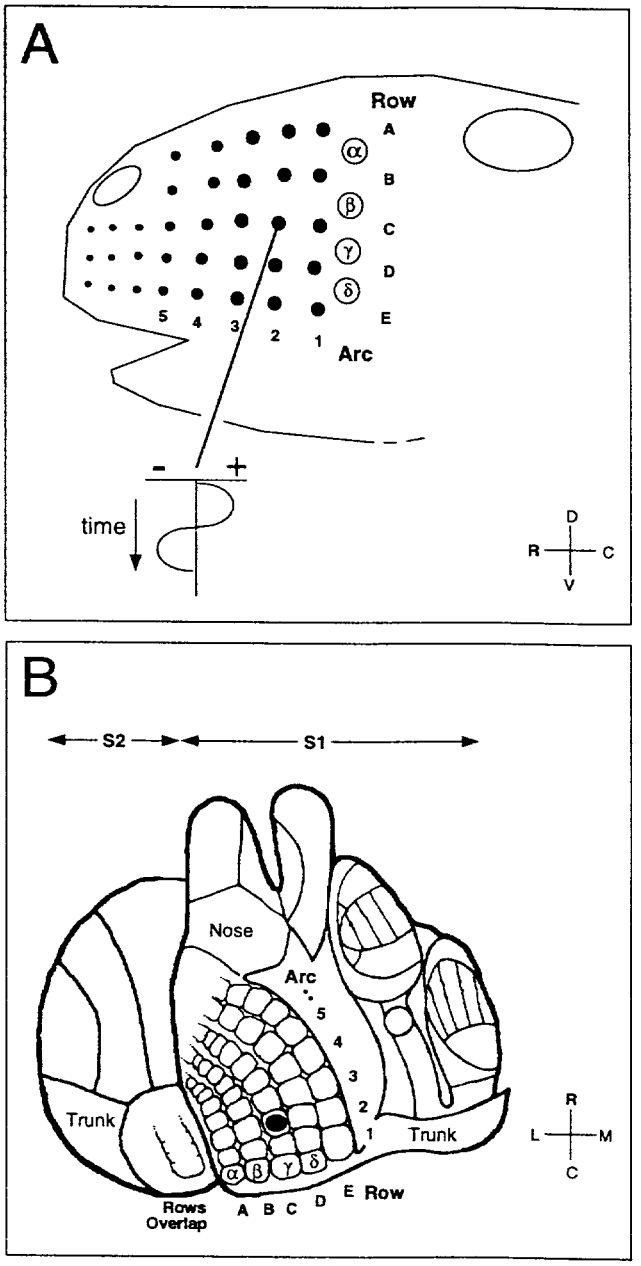


Fig. 1. Representation of vibrissa location in the mystacial pad of the rat and corresponding representation of the classic receptive field for each vibrissa in somatosensory cortex. **A:** Vibrissa location, drawn for the left side of the animal, with each vibrissa identified by its (row, column) address. The plot for the displacement of whisker C2 shows the motion of the stimulus that was used in these studies. R, rostral; C, caudal; D, dorsal; V, ventral. **B:** The central representation of each vibrissa in primary (S1) and secondary (S2) somatosensory cortex as drawn for the right (contralateral) side of the animal; a third somatosensory region that lies lateral to S2 (Krubitzer et al., 1986; Fabri and Burton, 1991) is not drawn. The solid circle corresponds to the representation of C2. The diagram is adapted from Chapin and Lin (1984), Carvell and Simons (1987), and the data shown in Figure 10.

unit studies (Chapin et al., 1981; Armstrong-James and George, 1988)? 4) Is the cortical response modulated by sustained stimulation of a vibrissa? 5) Is the pattern of the layer 2/3 response to motion of a given vibrissa modulated by motion of other vibrissae, as has been shown for single-unit activity in deeper cortical layers (Simons, 1985)? Preliminary aspects of this work have been published previously (Delaney and Kleinfeld, 1994; Kleinfeld and Delaney, 1995).

## MATERIALS AND METHODS

### Preparation

Fifty-seven Sprague-Dawley rats, aged P10 through P21 and of either sex, obtained from Camm Research Animals (Wayne, NJ) and housed locally, were subjects for this study. In preparation for recording, animals were anesthetized with a low dose of ketamine (50 μg/g body weight) that was supplemented with halothane (1–2% in $O_2$ at a flow of 500–1,000 SCCM); the ketamine was never supplemented. Body temperature was monitored and maintained at approximately 36°C. Once a plane of deep anesthesia was confirmed, an approximately 5 × 5 mm bone flap above parietal cortex was removed, followed by microdissection of the dura.[1] The cortex was bathed with a modified artificial cerebrospinal fluid (ACSF) that consists of 125 mM NaCl, 5 mM KCl, 10 mM glucose, 10 mM HEPES buffer, 3.1 mM $CaCl_2$, and 1.3 mM $MgCl_2$, pH 7.4. The care and experimental manipulation of our animals were in strict accordance with guidelines from the National Institutes of Health (1985) and have been reviewed and approved by a local institutional animal care and use committee.

### Staining

The cortex was stained with RH-795 (Grinvald et al., 1994; No. R-649; Molecular Probes, Eugene, OR) prepared as a 1 mg/ml solution in ACSF. We saturated a piece of gelatin sponge (Gelfoam; Upjohn, Kalamazoo, MI) with 50–100 ml of the dye solution, gently placed it on the exposed region of cortex, and covered it with a film of Parafilm to prevent evaporation. The cortex was stained for 1–1.5 hours, after which the surface was washed with ACSF and the skull of the animal was cemented to a stainless steel frame with dental acrylic. The cortical surface was coated with a thin layer of 0.5% (w/v) low-melting-point agarose (No. A-9793; Sigma, St. Louis, MO), and the frame was then filled with 1.5% agarose and sealed with a cover glass across the metal frame; care was taken not to compress the brain and compromise blood flow through the surface vasculature. Finally, the frame was attached to our recording apparatus to stabilize the head of the rat.

The distribution of dye throughout the cortex was assayed by examining thin sections of stained preparations. Six to seven hours after the onset of staining, the anesthesia was supplemented with pentobarbital (0.25 mg/g body weight), and the animal was perfused transcardially with 100 mM phosphate buffer. The brain was removed, blocked, immersed in a 1 ml aliquot of fresh egg white, rapidly frozen in isopentane chilled in dry ice, transferred to a Bright cryostat (Hacker, Fairfield, NJ), sectioned at 8 μm along the coronal plane, and thaw mounted onto No. 1 glass coverslips, and the extent of staining was visualized. As illustrated for a particular P17 animal, nearly uniform staining within the first 300 μm below the surface was observed (Fig. 2A), which was localized to fine processes and was essentially absent in profiles (Fig. 2C) that could be identified as neurons on the basis of their size after counterstaining with cresyl violet (data not shown). Measurement of the total fluorescence along a radial strip (n = 3)[2] showed that the staining fell to one-half its intensity at the surface by 600–700 μm (Fig. 2B). Thus, the upper part of layers 2/3 were well stained and would be expected to contribute to the optical signal. Of parenthetical interest, cell bodies deep to layer 6 exhibited punctate staining (Fig. 2D, and at asterisk in Fig. 2B); this suggests that an unknown population of cells or their afferents actively transports the dye.

### Optical measurements

We recorded changes in the fluorescent yield from the cortical surface of preparations stained, as described above, with a voltage-sensitive dye. The head of the rat was positioned so that the center of the cortical region of interest was held normal to the optical axis. The abdomen rested on a small, heated platform. Animals were maintained near stage III-3 anesthesia with halothane (1.0–1.5% in $O_2$ at a flow rate of ~ 500 SCCM). Body temperature was monitored and maintained between 36.4°C and 37.0°C. The animals received ip injections of 5% (w/v) glucose in physiological saline hourly (10 ml/g body weight), and to minimize respiratory distress they receive sc injections of atropine (10 μg/g body weight) hourly.

The technical constraints of current imaging technology preclude the use of awake animals. With regard to the present study, an advantage of anesthesia is that efferent activity in layer 1 was suppressed (Arezzo et al., 1981); thus, the interpretation of the optical signals was simplified.

***Apparatus.*** The optical apparatus is of local design and permits large areas, up to 5 mm in diameter, to be uniformly illuminated and imaged at ×0.5 to ×1 magnification with high efficiency. The sensitivity of our measurements was maximized by illuminating the cortex at the long-wavelength edge of the absorption spectrum of the dye ($\lambda$ ~ 520–560 nm for RH-795) and collecting the fluorescent light from the long-wavelength edge of the emission spectrum ($\lambda$ > 600 nm for RH-795). In practice, we illuminate at 550 ± 5 nm (mean ± half-width-half-maximum) at a typical intensity of 2 mW/cm$^2$; the illumination was gated to occur only while data are acquired. The emitted light was long-pass filtered at 610 nm and imaged onto a charge coupled device (CCD) with 0.5 numerical aperture optics.

The CCD camera (model CH250, with Thomson 7883 detector, 500 kHz 12-bit analog-to-digital converter and PC interface; Photometrics, Tuscon, AZ) operates in frame-transfer mode under the control of a Microsoft Windows-

[1]The dura may be tugged during removal of the flap, apparently by fine attachments to the overlying skull. This can lead to transient swelling that typically resolves within 10–15 minutes. We found that residual swelling compromises the optical signal, particularly those aspects away from the center of the response. We cannot overemphasize the fact that even the slightest nick to the cortical surface will compromise the signal.

[2]To the extent that the profile of stain vs. depth represents diffusion of the dye, a possibility not inconsistent with the roughly Gaussian shape of the fall-off (Fig. 1B), the effective diffusion constant for RH-795 in cortex is D ~ 5 × 10$^{-9}$ cm$^2$/second. This extremely small value may result from the formation of large micelles by the amphipathic dye molecules; it might be possible to increase D by mixing the dye with small detergent molecules.

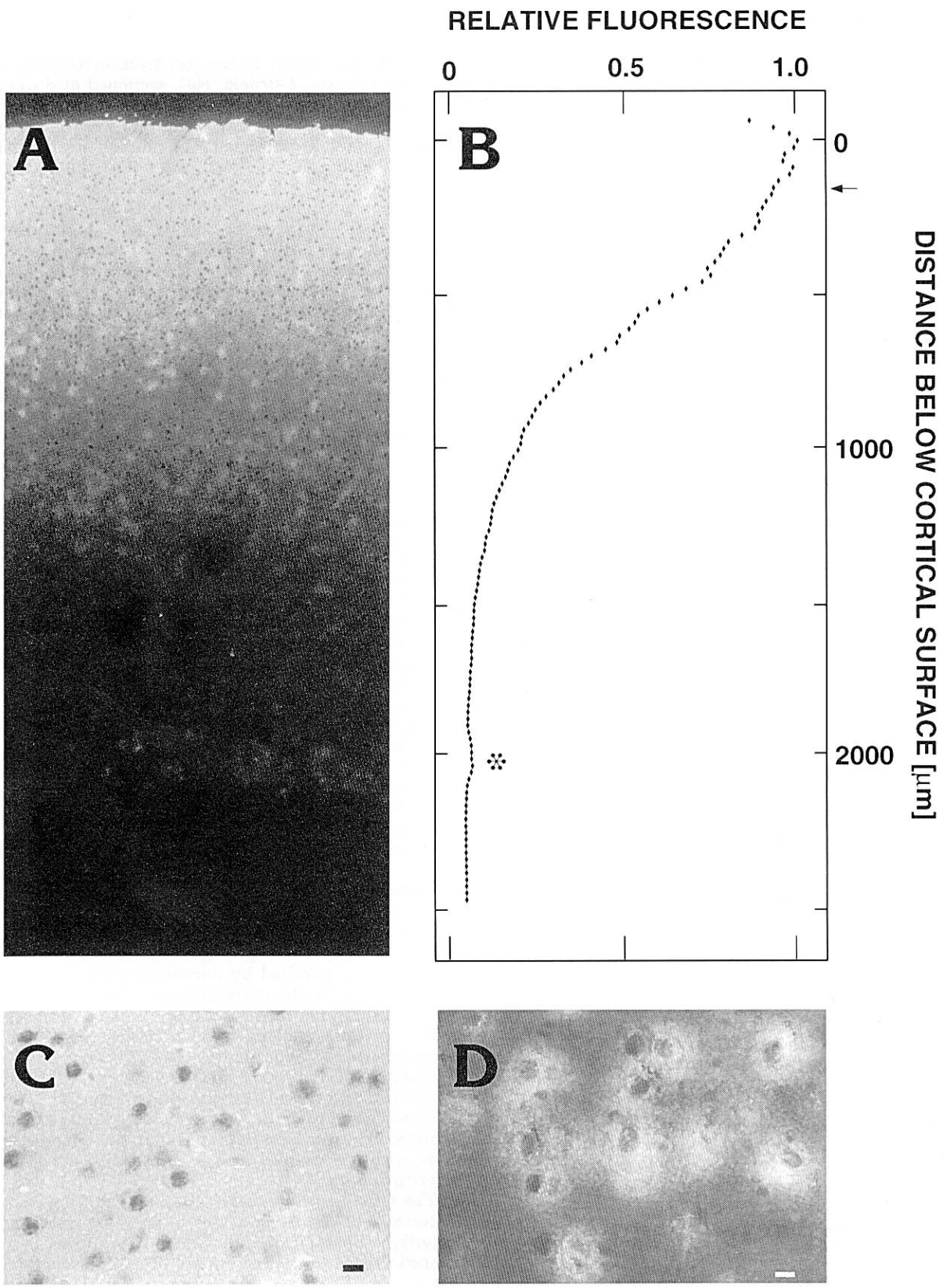


Fig. 2. Histological analysis of cortical tissue from a P17 animal stained with RH-795 for 2.0 hours. Sections are prepared along the coronal plane, as described in Materials and Methods. **A:** Low-magnification fluorescent photomicrograph. Note the high level of staining near the pial surface and the decline in staining with depth. A band of cells in layer 6 is also stained. The scale is given by the ordinate in B. **B:** Fluorescent intensity as a function of depth measured for the section adjacent to that shown in A. Note that the staining is essentially unchanged at the level of our focus depth (arrow; 200 μm) and the slight increase in intensity at the level of the stained, deep cells (*). **C:** High-magnification photomicrograph of stained processes and unstained somata at a depth of 200 μm relative to the pial surface. **D:** High-magnification photomicrograph of somata 200 μm deep. Scale bars = 10 μm.

based program of local design. Consecutive images of the entire field, with a scale of 22 μm per pixel for unity magnification, were typically acquired at frame rates up to 18.5 Hz for an 80 × 80 pixel image. Images were analyzed with the Interactive Display Language (Research Systems, Boulder, CO) graphics package run on a Sparcstation 10/41 (Sun Microsystems, Mountain View, CA).

The intensity of emitted light at time $t$ for a CCD element centered at location (x,y), where x, y, and t are discrete variables, is denoted $F(x,y,t)$. The spatially averaged change in transmembrane voltage within the field of each pixel, $\Delta V(x,y,t)$, is linearly proportional to the fractional change in emitted light,

$$\Delta V(x,y,t) = \alpha \frac{F(x,y,t) - \langle F(x,y,t)\rangle}{\langle F(x,y,t)\rangle} \equiv \alpha \frac{\Delta F(x,y,t)}{F(x,y)}$$

where $\alpha$ is a constant of proportionality and $\langle \cdots \rangle = T^{-1} \int_0^T dt$, in the present case, the baseline value of fluorescence for each pixel, $F(x,y) \equiv <F(x,y,t)>$, is determined from frames recorded prior to simulation of the animal, $T \leftarrow T_{pre}$. For cortical neurons in brain-slice preparations $\alpha \sim 10^4$ mV (Grinvald et al., 1994; Yuste, Tank, and Kleinfeld, unpublished observation ).

***Suppression of physiological noise sources.*** The pulsation of the brain with each cardiac cycle leads to a change in the fluorescent signal, of magnitude $|\Delta F/F| > 10^{-3}$, which constitutes the largest contaminant of our measurements on a single-trial basis. We minimized this contribution in three ways. First, physical motion of the cortex was reduced by embedding the exposed cortical region in an agarose-filled chamber, as described above, and suspending the chest of the animal to minimize artifacts caused by breathing. Second, the cardiac contribution to the fluorescent signal was used as a reference for the start of data acquisition. A small fraction of the total fluorescence from the cortex was split from the main optical axis, detected and filtered in a frequency band centered at the heart rate; the resultant signal corresponds to the first harmonic of the spatially averaged cardiac contribution to the change in fluorescence. Data acquisition alternated between positive and negative slopes of the zero crossings of the trigger signal. The cardiac contributions are suppressed across each pair of trials, typically by a factor of 2–3, within the correlation time of the heart rhythm; this time is ~4 seconds ( ~ 20 heart beats). Third, to remove the remaining cardiac contribution, as well as contributions from respiration, we subtracted a reference, denoted $\Delta F_R(t)/F_R$, from each pixel in the sequence of images. The reference was derived from the intensity of the image within an unresponsive region of cortex. We determined the fraction of the reference waveform that contributed to the optical change at each pixel with least-squares minimization; the corrected value of the optical change is

$$\frac{\Delta F(x,y,t)}{F(x,y)} \leftarrow \frac{\Delta F(x,y,t)}{F(x,y)} - C_{RS}(x,y)\frac{\Delta F_R(t)}{F_R}$$

where $C_{RS}(x,y)$ is the normalized overlap at each pixel, i.e.,

$$C_{RS}(x,y) = \frac{\langle \Delta F(x,y,t)\Delta F_R(t)\rangle}{\langle \Delta F^2(x,y,t)\rangle}\frac{F_R}{F(x,y)}$$

and the time averaging is over the entire sequence of images. This final scheme reduces the cardiac component of the signal by an additional factor of 2 or less; incomplete cancellation results from spatial differences in the phase of the pressure wave across the cortical surface.

***Resolution.*** The transverse resolution of our measurements depends on the contribution to the optical signal from out-of-focus fluorescence. We determine this contribution from images of a small crystal of dye that is lowered into perfused but fresh brain from juvenile (P14) rat. The size of the crystal, ~20 μm on edge, was approximately equal to the lateral resolution per pixel at unity magnification. The focus of the objective was fixed just below the cortical surface, and the amplitude of the optical signal in the pixel centered with respect to the crystal was plotted as a function of depth relative to the focal plane. The intensity was observed to fall off with a half-width at half-maximum of $\sigma \sim 80$ μm (Fig. 3A), and the transverse resolution is $\sqrt{\sigma} \sim 120$ μm. A similar value of $\sigma$ was observed in ACSF (data not shown), which implies that scattering from tissue in the upper layers of neocortex was not significant for our measurements. To illustrate this graphically, we observed essentially no difference between a focused image of the crystal taken in air vs. 1,000 μm deep to the cortical surface (Fig. 3B); this depth was far greater than the 100–200 μm depth of interest in this study.

Signal-to-noise constraints, dictated ultimately by the capacity of each electron well in the CCD camera, forced us to spatially average our final images, in addition to trial averages and possibly frame (time) averages. Each map was spatially filtered by convoluting the original image with a rectangular window, 7 pixels on edge unless otherwise noted; for unity magnification, this corresponds to a lateral resolution of ~80 μm.

Finally, we set our focus 100–200 μm below the cortical surface. Although the curvature of the brain along the lateral-medial axis causes the depth to be less at the edges of the image than at the center, this choice of focus implies

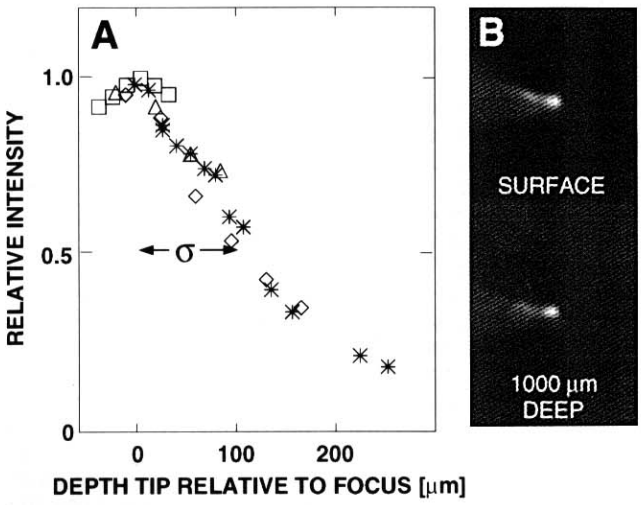


Fig. 3. Optical properties of cortex from a P20 rat that was freshly perfused with phosphate-buffered saline. **A:** Relative intensity in a pixel centered above a 20 μm crystal of dye embedded in a glass pipette tip with the focus held fixed and the crystal lowered below the cortical surface. Each pixel images a 22 × 22 μm region. **B:** Images of the crystal in air and at a depth of 1,000 μm below the cortical surface. Note that there is essentially no blur in the focused image of the crystal deep in cortex.

that our data were collected primarily from the upper part of layers 2/3.

## Stimulation

One or more vibrissae were stimulated with piezoelectric "wigglers," constructed from 1.5 × 0.160-inch parallel-connected bimorph (No. PZT-5H; Morgan Matrox, Electroceramic Division, Bedford, OH), as described elsewhere (Simons, 1983), with a 0.3-mm-diameter graphite rod to connect the bimorph to a sleeve that captures a vibrissa. The resonance frequency of the assembly was between 90 and 100 Hz. The bimorphs were driven in the rostral-to-caudal-to-rostral direction by a tone burst generator whose output was filtered at $f_{3dB}$ = 60 Hz with an eight-pole Bessel filter and amplified. Individual vibrissa were typically stimulated with 20 Hz or 40 Hz tones, and groups of vibrissae, threaded through nylon screen (20 mesh/inch) rather than a sleeve, were stimulated with a 20 Hz tone.

## Electrical measurements

Extracellular measurements were made with some preparations after the completion of all optical recording. The glass that forms the top of the recording chamber was removed, a Parylene-coated tungsten electrode (No. WE300310A; Micro Probe, Clarksburg, MD) was aligned to lie radial to the surface, and the vasculature on the exposed cortical surface was used to position the electrode relative to the location of the relevant optical signal. Penetrations were made to a final depth of 600–700 μm below the pia, approximately the depth of layer 4. The electrical signals were band limited between 400 Hz and 10 kHz (four-pole Bessel filter), the largest unit was selected with a window detector (Palmer and Davis, 1981), and the unit arrival time was recorded with software of local design. The depth of penetration was confirmed by electrolytic lesion (−15 μA for 15 seconds), which was located in 200-μm-thick coronal sections of the brain.

## Histology

The location of the underlying afferent projections, i.e., the layer 4 barrels, was determined from sections stained for cytochrome oxidase. The animal was anesthetized with pentobarbital, perfused transcardially with 100 mM phosphate buffer followed by 0.8% paraformaldehyde in phosphate buffer, and decapitated; the top half of the skull was removed, and the white matter that underlies neocortex was cut with forceps to the level of the rhinal sulcus. The brain was then removed, the dissection of the neocortex was completed, and pinholes were made normal to the surface as alignment marks. The tissue was flattened between microscope slides spaced 2.0 mm apart and stored for up to 2 weeks in 0.8% paraformaldehyde in phosphate buffer at 4°C. Seventy-micrometer-thick sections parallel to the surface were prepared with a Vibratome (Stolting, Wood Dale, IL) in which the mounting chuck was replaced with a dual-axis tilt stage (No. 485; Newport, Irvine, CA) so that tissue could be oriented to lie parallel to the cutting plane. After cutting, sections were stored in 0.8% paraformaldehyde in phosphate buffer for 1–20 hours.

Our procedure for staining is modified from that of Liu et al. (1993). Sections were washed twice in 100 mM phosphate buffer and once in 100 mM Tris buffer, pH 7.4; incubated for 2–10 hours at 37°C in a cocktail of 9 μM horse-heart cytochrome *c*, 640 μM 3,3′-diaminobenzidine, 15 mM $NiSO_4$, and 110 mM [4% (w/v)] sucrose in 100 mM Tris and 100 mM imadazole buffer, pH 7.4, at T = 37°C; washed in 100 mM phosphate buffer; fixed with 4% paraformaldehyde in phosphate buffer; washed in buffer; washed in distilled water; and mounted. Cytochrome oxidase-rich regions at the level of layer 4 are aligned relative to the surface vasculature in the top section. This vasculature was also seen in the in vivo optical images, $F(x,y,t)$, and thus acts as a fiducial to fix the anterior-posterior axis.

# RESULTS

## Optical signal: Sensitivity issues

Motion of one or more vibrissae leads to stimulus-locked changes in the optical properties of vibrissa cortex. As a prelude to the interpretation of our results, we consider three issues related to the origin and repeatability of the optical signal.

***Dye related vs. intrinsic signals.*** The fluorescent image of the cortex will contain a contribution from intrinsic changes in the optical properties of cortical tissue and a contribution that emanates specifically from changes in the optical properties of the dye associated with electrical activity. These two contributions are separable in time; the onset of the dye-related signals occurs concurrently with afferent activity (Orbach et al., 1984), whereas the onset of the intrinsic contribution lags behind the onset of stimulation by ~1 second and recovers to baseline over a period of 10 seconds or more (Grinvald et al., 1986). Here we examine whether there are stimulus conditions that excite the dye signal, and not the intrinsic signal, as a means of simplifying the interpretation of our signals.

A cluster of vibrissae were stimulated with sinusoidal motions of different magnitude at 20 Hz. For brief, weak stimulation, i.e., 80 milliseconds or five cycles of ±2°, we observed an optical signal that rose with the onset of stimulation, peaked after about 150 milliseconds, and decayed with a time constant of ~150 milliseconds (Fig. 4A,C). There was no late component. Two additional features were resolved when the duration of the stimulus was increased to 0.9 seconds. The first was an off-response upon cessation of the stimulus (asterisks in Fig. 3B,D). The second was a response that rose after a delay of 1.5 seconds and that recovered only very slowly in time (Fig. 4B,D). The magnitude of the late response was increased, and its apparent latency decreased, by increasing the amplitude of the stimulus for vibrissa displacement to ±6° (Fig. 4E). Finally, only the long-latency signal is observed in preparations that are not stained with dye (data not shown), consistent with known results (Grinvald et al., 1986).

We associate the prompt signal with cortical depolarization that is reported by the voltage-sensitive dye and associate the delayed signal with activity-dependent changes in the intrinsic optical properties of cortex. In all of our further studies, the stimulus was sufficiently brief and weak that it did not produce observable changes in the intrinsic properties. This ensures that the spatial patterns of activation we report reflect changes in the pattern of cortical depolarization, as opposed to reflecting possibly different patterns that result from changes in hemodynamics.

***Repeatability.*** We now consider the repeatability of the time- and trial-averaged optical signal observed in response to stimulation of a single vibrissa (n = 3). Qualitatively, averages of ~5 seconds (e.g., 16 trials of 300 millisecond integrated responses) suffice to establish the center and

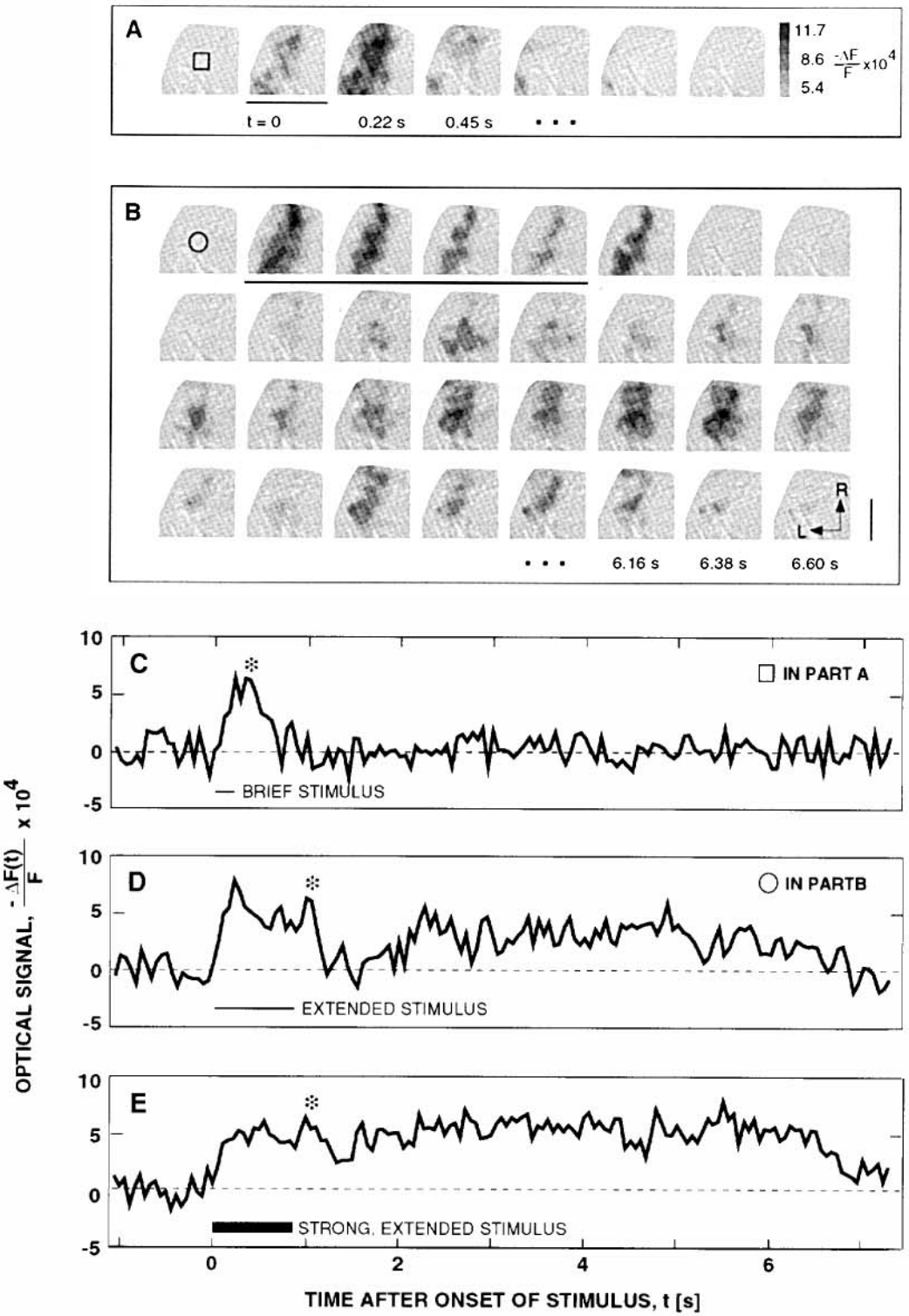


Fig. 4. Cortical response as a function of the strength of stimulation. A fine nylon mesh was used to stimulate simultaneously whiskers B1, B2, C1, C2, D1, D2, E1, and E2 with 20 Hz sinusoidal deflections, with amplitude and duration given below. **A:** The response to weak, brief stimulation, i.e., four cycles at ±2°, that occurred within the time course of the first image shown ($0 < t < 223$ milliseconds; solid line). Note the complete recovery after the cessation of the stimulus and the possible off response (asterisk in C). Each image is 100 × 100 pixels; four consecutive CCD frames (55.7 milliseconds per frame) are summed and eight trials are averaged (1.8 seconds total). The change in fluorescence is quantitized in steps of $\Delta F/F = 1.55 \times 10^{-4}$ and is plotted above a muted version fluorescent image of the cortex. Scale as in B. **B:** Response to weak, prolonged stimulation, i.e., 16 cycles at ±2° that occurred during the time course of the first four images ($0 < t < 891$ milliseconds; solid line). Note the partial recovery after the cessation of the stimulus, the off response (asterisk in D) and the presence of a new response that comes on long after the stimulus is off. Conditions as in A. Scale bar = 2 mm. **C:** Line plot of the response shown in A, averaged over an 11 × 11 pixel region centered over the center of the optical signal. Note the off response (asterisk) and the complete recovery of the response after cessation of the stimulus. **D:** Line plot of the response shown in B, averaged within the center of the response. Note the off response (asterisk), the partial recovery of the response after cessation of the stimulus, and the delayed rise and eventual recovery of a secondary response. This later signal is associated with stimulus-induced changes in the intrinsic optical properties of the cortex. **E:** Line plot of the response to a prolonged, strong stimulus, i.e., 16 cycles at ±6°. Other conditions as in D. Note the off response (asterisk) and the relatively large amplitude and sustained time course of the secondary response. Conditions as in D. P19 animal.

gross shape of the region of activation (averages of 16 trials; Fig. 5A), whereas averaging of ~20 seconds provides details of the shape on the ~100 μm scale (averages of 64 trials; Fig. 5A); the latter period corresponds to the practical maximum in many of our experiments. A semiquantitative analysis of the variability in the signal reveals that it is typically two to three times that given by the shot-noise contribution. The source of the extra variability is dominated by our inability to correct for all sources of physiological noise (see Materials and Methods) and may include additional components that reflect intrinsic trial-to-trial variability in the spatial pattern.

A second issue relevant to this study is the repeatability of the response over the time scale required to measure the response of many vibrissae; 20–30 minutes per vibrissa is typical. We observed that the position of the center of the response as well as details at better than a 200 μm scale were preserved when replicate measurements were taken 90 minutes apart (Fig. 5A).

***Effect of focus depth.*** We expected that the shape of the optical signal would not vary much for changes in focus depth on the scale of the transverse resolution, ~120 μm (see Materials and Methods; Fig. 3). These expectations were approximately borne out by experiment (n = 2), as shown by the successive images of cortical depolarization in response to stimulation of whisker E1 (Fig. 5B). We observed that the center of the response was unchanged as the focus depth was varied by ±150 μm relative to our nominal depth of 150 μm below the cortical surface. With respect to details of the shape of the optical signal, only a peripheral aspect of the response systematically decreases with depth (rostral edge in data shown in Fig. 5B), although part of this effect is caused by slow changes in the response over the time course of these measurements (Fig. 5A).

## Optical signal: Basic response

***Spatial pattern from stimulation of a single vibrissa.*** We focus on the time-averaged response induced by stimulation of a single vibrissa with a train of low-amplitude sinusoids. As can be seen with a particular example for whisker D2, there is a central region that contains the maximal response along with a number of local maxima that we have denoted as "satellite" regions (Fig. 6). The satellite regions are spaced so that they may lie above neighboring column; we return to this issue below (see Fig. 14). The spatial extent of the optical signal depended on the choice of threshold level, although this effect was weak when the level was chosen to just encompass the satellites. For the example shown in Figure 6, the response extends ~0.9 mm for a level that includes the satellites but little background (70% or maximum for this example); this extent increased to 1.2 mm when the level was decreased to include satellites and appreciable background (50% of maximum).

The large spatial scale of the optical signal (~1 mm; Fig. 6) relative to the ~300 mm scale of the layer 4 barrel was, details aside, typical of all cases studied (n = 50). The

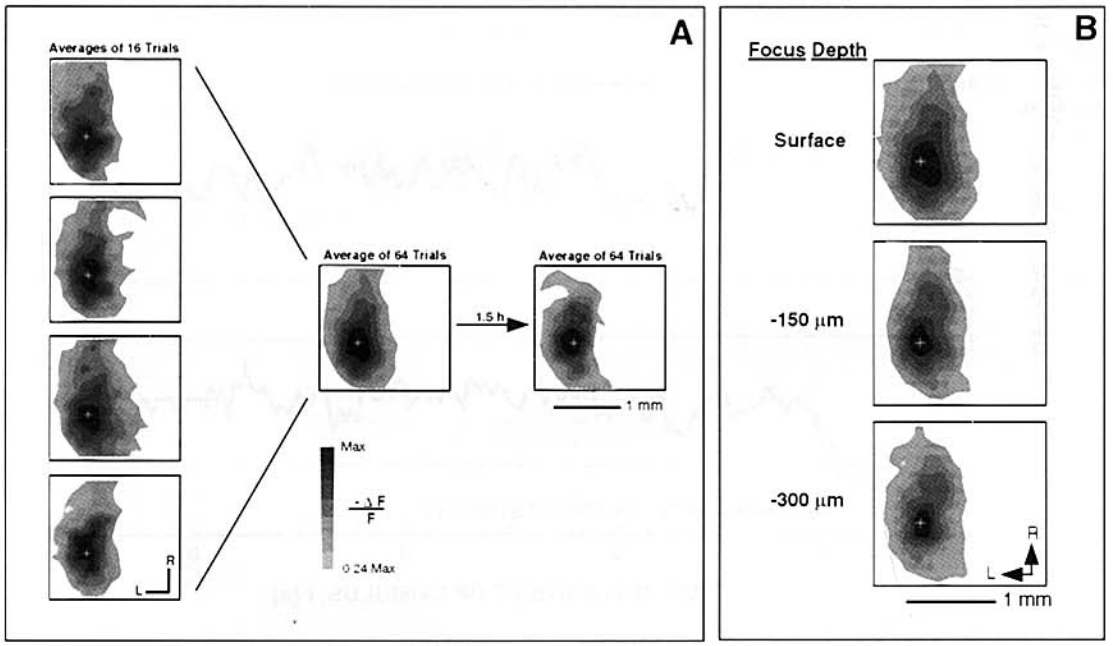


Fig. 5. Sensitivity issues. **A:** Repeatability of the optical signal. Whisker E1 was stimulated for eight cycles at 43 Hz, and each signal is the average over five frames (285 milliseconds). We plot the depolarization, thresholded at 25% of the maximal amplitude, as an eight-level gray scale. The plus sign is an invariant position marker, and the focus in this series is at the surface. The responses in the column at left are the average of 16 consecutive trials (4.6 seconds of data), i.e., 64 trials in total. The results from four such consecutive measurements serve to illustrate the repeatability of the signal; the maximal values of the four signals are $-\Delta F/F$ = 0.0010, 0.0009, 0.0012, and 0.0009, respectively. The response in the center comprises all 64 trials shown at left; it should be compared with a similar measurement made after an interval of 90 minutes; the maximal amplitudes of the two signals are $-\Delta F/F$ = 0.0010 and 0.0006, respectively. These latter data illustrate the repeatability of the signal over time. **B:** Spatial extent of the optical signal as a function of the depth of focus relative to the cortical surface. Stimulation of whisker E1 and data collection as in A; the data for the time series in A span the interval over which the data for the depth series were taken. We show the response averaged over 64 trials (18.5 seconds total). The maximal amplitudes of the three signals are $-\Delta F/F$ = 0.0010, 0.0008, and 0.0008, respectively. P12 animal.

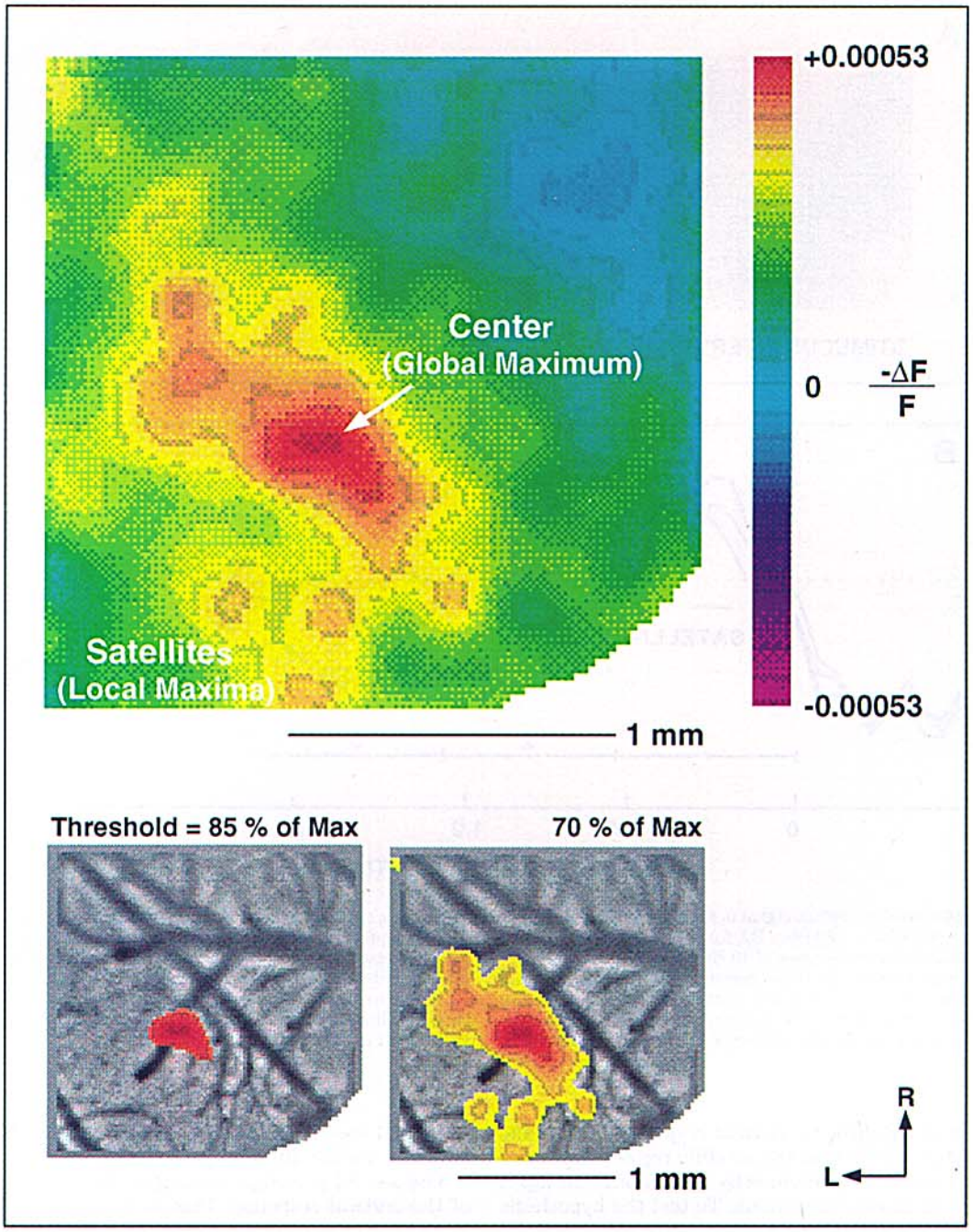


Fig. 6. Detailed view of the cortical depolarization induced by a motion of a single vibrissa. Whisker D2 was stimulated for 10 cycles of 40 Hz sinusoids, ±2° amplitude, with one cycle every 57 milliseconds; the response is averaged over 800 milliseconds (14 frames) and 16 trials (12.8 seconds). Note the global maximum of the signal, denoted the center, and the multiple local maxima, denoted satellite regions. The images at bottom show the optical signal superimposed on a fluorescence image of the cortex and thresholded as noted. P17 animal.

shape of the signal in response to deflection of essentially any vibrissa that lies in rows C–E was crudely elliptical, with the long axis along the "row" direction (see also Fig. 11) and with an aspect ratio of 1.4 ± 0.4 (mean ± SD; n = 37); the deviation from isotropy is significant at the level of 6σ (σ = SD/√n, the standard deviation of the mean). In contrast to the response for vibrissae in the ventral rows, stimulation of straddlers β, γ, or δ led to responses that showed no systematic pattern of elongation (aspect ratio of 0.9 ± 0.2 with respect to the "row" direction; n = 7), although they also showed both epicenter and satellite regions (Figs. 6, 11). Finally, stimulation of vibrissae in row B consistently yielded fragmented cortical responses (n = 3; see, e.g., Fig. 11), as opposed to the contiguous responses seen for stimulation of vibrissae in rows C, D, and E and the straddler column.

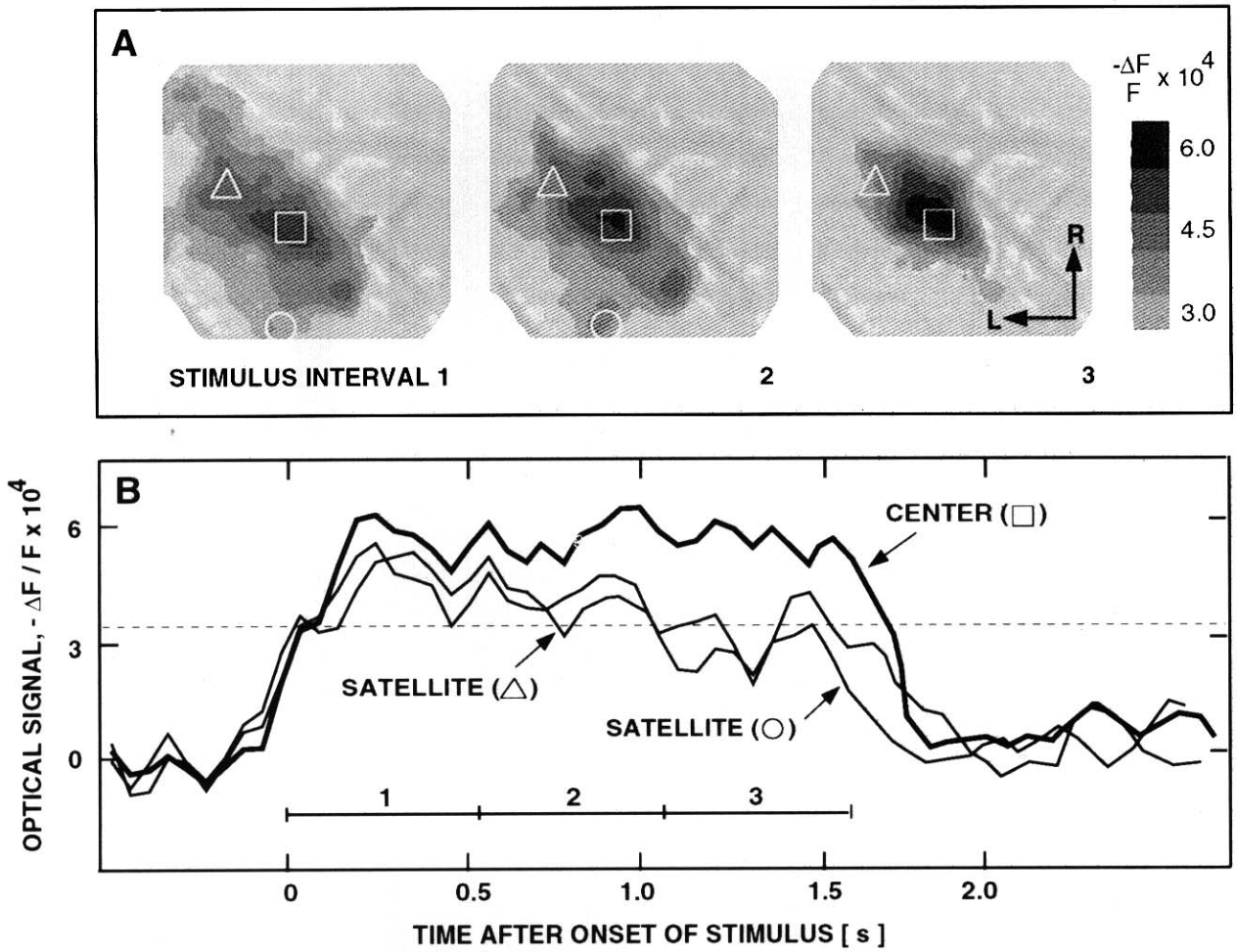


Fig. 7. Adaptation of the optical signal in satellite vs. central regions with continuous stimulation. Whisker D2, for the same rat as shown in Figure 5, is stimulated with 30 cycles of 40 Hz sinusoids, ±2°, with one cycle every 57 milliseconds (the frame period), over an interval of 1.6 seconds. The data shown are averaged over 32 trials. **A:** Successive maps of the depolarizing response shown overlying the surface vasculature, averaged over successive 460 milliseconds (nine frame) intervals. The map is thresholded at 45% of the maximal response. **B:** Plot of the time dependence of the response in the central region (squares in A) and satellite regions (circles and triangles in A) of the cortical response. The intervals labeled 1, 2, 3 correspond to the 460 millisecond intervals used to construct the maps in A. The dashed line corresponds to the threshold level used for the maps. The curves have been smoothed by a three-point uniform filter.

***Adaptation of satellite vs. central responses.*** We take as a working hypothesis that the satellite regions represent activation of neighboring columns by weaker afferent input and local intralaminar connections. To test the hypothesis further, we compared the temporal structure of these regions using sustained vibrissa stimulation and considered two paradigms to detect adaptation of the response that were appropriate for the ~50 millisecond time resolution of our optical instrumentation.

The first paradigm considered "short-term" adaptation of the response in the central vs. satellite regions of the signal. We stimulated a given vibrissa with low-amplitude deflections for the relatively extended period[3] of 1.6 seconds. As is illustrated for the case of D2 (Fig. 7A), the optical signal averaged over the first ~500 milliseconds shows the central and satellite regions presented above (Fig. 6). At longer times, the amplitude at the center of the response remained essentially constant, whereas that in the satellite regions decayed (Fig. 7B). The rate of decay, on the order of 1 second, is the same for different satellite regions (Fig. 7B) and for different preparation (n = 5).

The second paradigm considers "long-term" adaptation of the cortical response. This is examined by "driving" a vibrissa with prolonged, repetitive deflections and recording the cortical response when the vibrissa is probed with single, transient deflections. There are two controls. First, we assay the response of "driven" vibrissa after a long recovery time. Second, we compare the response of the "driven" vibrissa with a naive "control" vibrissa to ensure that the overall electrical responsiveness of the cortex is

[3]Simons (1978) examined the response of cortical cells driven by excitation of their principal vibrissa for 1 second with sinusoids of frequencies up to 40 Hz, the highest frequency used in this study. There was essentially no adaptation of the response for both rapidly spiking units, presumably interneurons, and regular spiking units, presumably pyramidal cells. The time course in response to stimulation of neighboring vibrissae was not reported.

stable. In detail, the sequence of steps is as follows (Fig. 8). 1) We first obtain baseline spatial patterns in response to a brief train of sinusoidal deflections applied either to the "driven" or to the "control" vibrissa. To minimize systematic errors, the time between trains is long, i.e., 30 seconds, and trials for the two vibrissae are interspersed. 2) To test for adaptation, the "driven" vibrissa is stimulated 100 times, with an interstimulus interval[4] of 2 seconds, with the same sinusoidal deflections used for the baseline determination. At the end of this episode, we measure the spatial pattern for the "driven" vibrissa only in response to trains spaced every 30 seconds, as in the baseline measurements. 3) To determine the time course and stability of the adaptation, the paradigm (step 2) is repeated three times. 4) We measure, as a control for drift in the cortical response, the spatial pattern for the "driven" and "control" vibrissae with stimulation procedures identical to those used in the establishment of the baseline. Approximately 1,500 seconds has passed since the baseline measurements. 5) To establish recovery of the response for the "driven" vibrissa, and as an additional control for possible drift in the response (Fig. 5A), we allow the rat to recover for an additional 1500 seconds, after which we measure the spatial pattern for the "driven" and "control" vibrissae.

We chose vibrissae whose optical signals in response to stimulation are well separated and consider the particular example of whisker b as the "driven" vibrissa and C3 as the "control" (Fig. 8). By design, little signal averaging could be performed in this experiment, and the peak-to-peak signal-to-noise ratio is 2. Nonetheless, we observed that the width of the spatial pattern of β decreased in extent with continued stimulation, from >1,400 μm to 600 μm (spatially averaged full-width half-maximal response). The decrease reaches its steady-state level essentially within the first stimulation period, or 200 seconds. After the recovery period, the width returns to near its original value (>1,200 μm). In contrast, the size of the spatial pattern for the "control" changed relatively less after continued stimulation of β and actually became slightly broader rather than narrower.

To quantify the above-described adaptation effect across separate experiments, we chose a threshold level that included the satellites in the prestimulation data and measured the average change in area of the signal lying above this threshold level relative to the average area of the prestimulation and recovery values (i.e., the average area from steps 2–4 divided by that in steps 1 and 5; Fig. 7). We observed a fractional *decrease* to 0.35 ± 0.20 (mean ± SD; n = 4) of the initial area for the "driven" vibrissa; in contrast, the "control" showed an *increase* to 1.35 ± 0.20 (mean ± SD; n = 3) of its initial value.

The results from the first paradigm show that continuous stimulation leads to adaptation of the response in satellite regions but not in the central region (Fig. 7). The result from the second paradigm shows that even weak stimulation leads to diminution of the cortical response and is consistent with adaptation of the satellite but not central regions (Fig. 8).

***Time course for a single vibrissa deflected once.*** The time course of the onset of the cortical response was measured for individual vibrissae that were stimulated with a single sinusoid, with the caveat that considerable trial averaging was required, typically 100 trials. We observed spatially localized cortical depolarization (Fig. 9A,B) whose eventual recovery time was similar to that observed with continuous stimulation (Fig. 4C). In addition, we noted that the onset of the response was followed by a transient dip in amplitude (Fig. 9A,B) that occurred 100–200 milliseconds after the onset of the depolarization. This is suggestive of transient inhibition that follows the initial excitation, although the dye signal does not allow one to discriminate among solely excitatory vs. mixed excitatory-

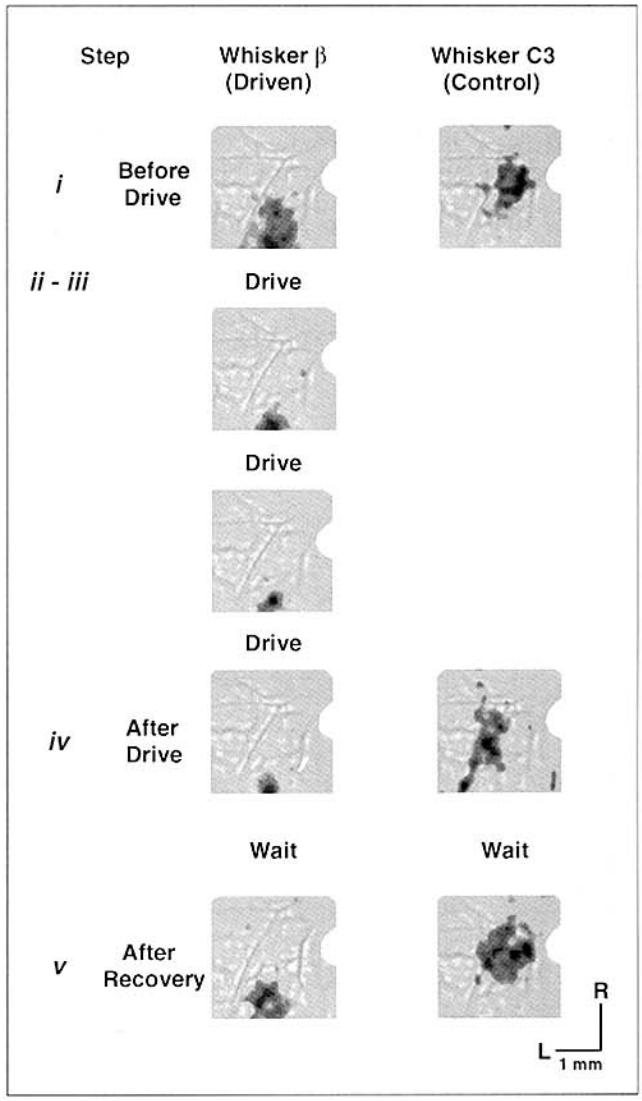


Fig. 8. Adaptation of the optical signal with prolonged but intermittent stimulation. Conditions as described in the text (steps 1–5; stimulus is six cycles of 20 Hz sinusoids of ~ ±3°, and each datum is the average of eight trials. For individual trials, the vibrissa were stimulated for 250 milliseconds and the response was integrated for 400 milliseconds (3.2 seconds total average). The optical signal in each datum is normalized by the maximum depolarizing response and overlies an image of the cortex. Note the decrease in the extent of the depolarization caused by continuous movement of the driven vibrissa and that most of this decrease occurs after the first period of driven stimulation. P13 animal.

[4]We chose an interval time of 2 seconds to be long compared to the decay of the central response upon cessation of stimulation (~200 milliseconds; Fig. 8) and to ensure a low duty cycle (12%).

inhibitory inputs to a region. Direct support for an inhibitory component comes from measurements of the local field potential that is induced at the location of the optical signal. In response to deflection of a single vibrissa, as described above, we observed the rapid onset of an inward current, followed by a slower, outward current (Fig. 9C). These currents are consistent with the prompt excitation and delayed inhibition in the triphasic, excitation → inhibition → excitation, optical signal (Figs. 9A,B).

This time course, excitation → inhibition → excitation, was seen in all measurements of a single vibrissa displaced once. The average latency to the dip is 170 ± 50 milliseconds (mean ± SD; n = 9); the variation is likely to be dominated by sampling error. Note that the need for extensive trial averaging makes observation of more than a few such measurements impractical within a given set of experiments.

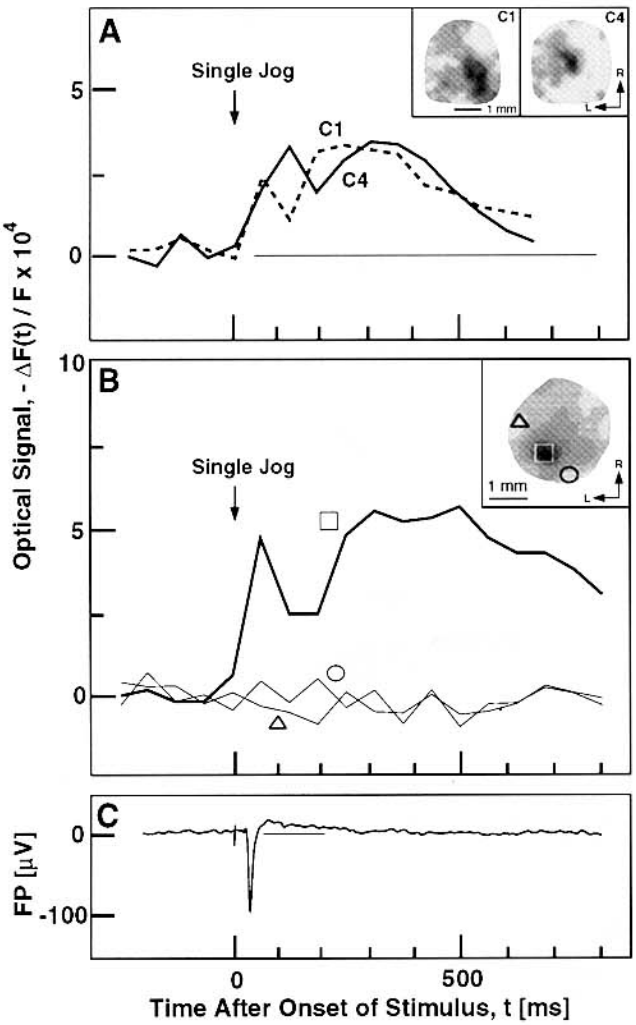


Fig. 9. Time course of the optical signal induced by a single cycle of sinusoidal motion applied to an individual vibrissa. **A:** Time plot shows the temporal response averaged over the central region of activation (**inset**) for whiskers C1 and C4 for the same animal. The stimulus is a single 40 Hz sinusoid of ~ ±2°, and the data are the average of 96 trials. Note the inhibitory dip at 115 and 170 milliseconds, respectively, for C1 and C4. P25 male rat. **B:** Temporal response averaged over the central region of activation (thick line; square in inset) and outside regions (thin lines; circle and triangle in inset) for whisker D1. The stimulus is a single 40 Hz sinusoid of ~ ±2°, and the data are the average of 128 trials. P17 male rat. **C:** Local field potential measured at a depth of between 550 and 600 μm over the region of central activation for whisker C3. The stimulus is a single 40 Hz sinusoid of ~ ±3°, and the data are the average of 34 trials. P20 animal.

## Spatial maps of the optical response

We now consider the relation of the spatial responses induced by activation of different vibrissae in the same animal.

***Simultaneous mapping of S1 and S2.*** We focus first on the representation of cortical responses induced by simultaneous displacement of vibrissae in columns 1–3 of a given row in a P14 animal. A broad response was observed following stimulation of rows E, D, C, or B that was elongated nominally along the rostral-caudal axis (top row, Fig. 10); this is consistent with the known anatomy of S1 (Fig. 1). The systematic activation of rows E–B, i.e., ventral-to-dorsal rows, produced a medial-to-lateral shift in the location of the optical signal; again, this is consistent with known anatomy. Furthermore, we observed a second, weaker set of bands (bottom row, Fig. 10) lying lateral to those in S1. In contrast to the shift in position for the bands in S1 upon systematic activation of rows E–B, these weaker bands were completely overlapped. We associate this response with the vibrissa representation in area S2 (Carvell and Simons, 1987), although possible activation of a third somatosensory area (Fabri and Burton, 1991) cannot be ruled out. Area S2 lies quite lateral in older animals, and, this being the case, the cortical signal was observed in our field of view only in our youngest animals (P10–P13; n = 3). In contrast to the case with activation of S2, we observed no activation of the dysgranular zone, which lies medial to S1.

***Single vibrissa maps of the central response in S1.*** The optical signals induced by displacement of individual vibrissae form an ordered map, whose typical features are shown in the example in Figure 11. We observed that the central regions for activation of whiskers D1, D2, and D3 form a line that runs diagonally across the cortical surface, consistent with the data in Figure 10 and with known anatomy (Fig. 1). Furthermore, the fields of activation defined by straddlers γ and β, whiskers D1 and C1, and whiskers D2 and B2 also form lines that run diagonally across the cortical surface (Fig. 11) but are perpendicular to the D1–D3 row direction. This is also consistent with known anatomy. Similar results were found with other animals (n = 7, with up to ten vibrissae represented in a map from one animal). Thus, a map of the central response of the optical signal appears isomorphic with the map of the location of vibrissa on the mystacial pad.

***Relation of single vibrissa maps to afferent input.*** The general features of the above-described map are consistent with a large volume of anatomical and electrophysiological data on the organization of the columnar fields for the vibrissa. Nonetheless, because the signals we observe are relatively broad (Figs. 6, 11) and because it is known that the organization of the barrel region varies between animals (Woolsey and van der Loos, 1970), we compared partial maps of our optical signals and two independently derived measures of the columnar organization. The first involves single-unit recording at the level of layer 4, a measure of monosynaptic activation by thalamocortical afferent. The afferent input to this layer is particularly

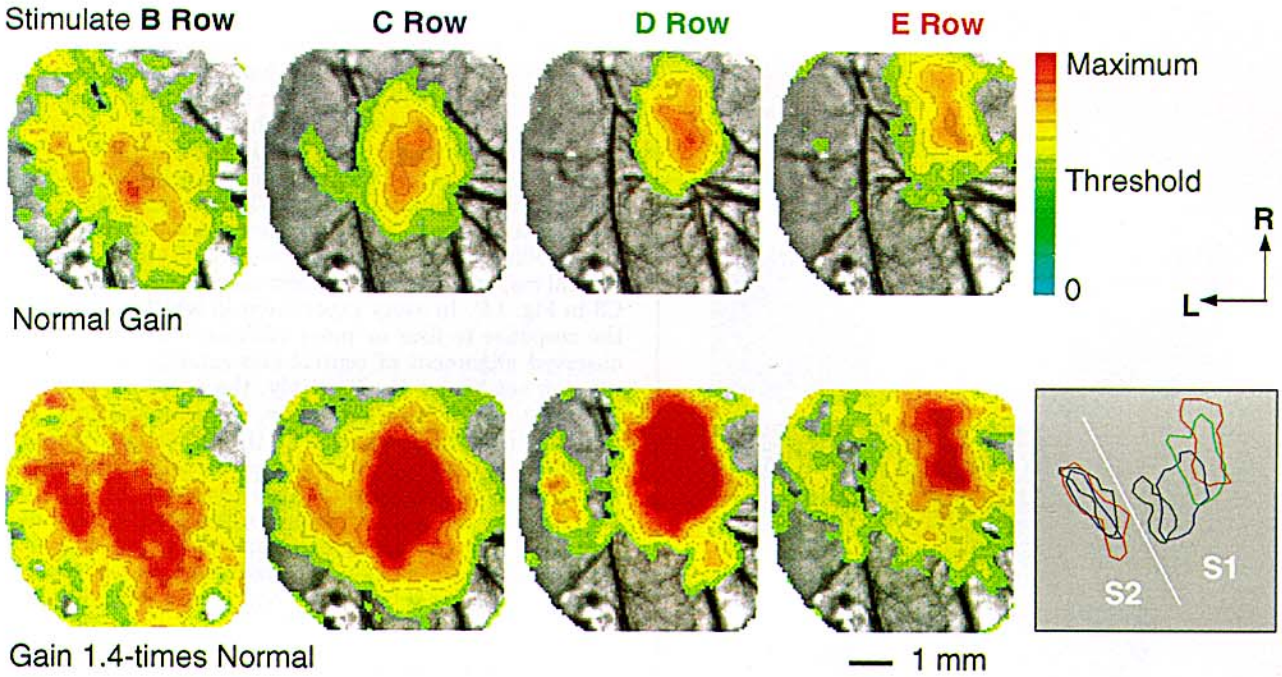


Fig. 10. Cortical response to synchronous motion of single rows of vibrissae. Columns 1–3 in a given row of vibrissae, either B, C, D, or E, were stimulated. We stimulated with 25 Hz sinusoids of ~ ±3° for six cycles (240 milliseconds). Each response is averaged over 662 milliseconds (eight frames) following the onset of stimulation and eight trials for row D and 16 trials for rows B, C, and E (5.3 seconds and 10.6 seconds in total, respectively). **Top:** Data displayed as an overlay of changes in depolarization, thresholded at 0.50 times the maximal change for that row, above the image of the surface vasculature. Note the shift of activation toward the lateral edge of cortex as the stimulation is moved from E to B row; this is associated with S1. The optical signal in each datum is normalized by the maximal depolarizing response and overlies an image of the cortex. **Bottom:** Data in A redisplayed with an expanded scale. Note the appearance of a second region of depolarization along the lateral edge for all rows. This is associated with S2. Box: Outlines of the optical response at the level of 75% of maximum for activation in S1 and S2. The color scheme of black, blue, green, and red signifies stimulation of rows B, C, D, and E, respectively. Note the complete overlap of response in S2. P10 animal.

strong for, although not limited to, the primary vibrissa for that cortical column (see, e.g., Armstrong-James et al., 1992). Thus, the receptive field delineated by unit activity in layer 4 defines the locus of afferent input. The second measure utilizes the preparation of tangential sections of cortex that are stained for cytochrome *c* oxidase. This enzyme, involved in the final step of respiration, is a measure of the high metabolic activity associated with afferent presynaptic terminals. Thus, sites of reaction product, denoted barrels, define loci of afferent input. For concreteness, we consider the correspondence between the optical signals and single-unit recordings in terms of the signals induced by stimulation of whiskers C1 and C2; the central responses of the optical signals are outlined in Figure 12A. With the electrode located at the center of the signal for C1 (1 in Fig. 12A), we mapped the receptive field for the largest unit(s) (Fig. 12B). There was a strong, punctate response induced by stimulation of C1, a weak response induced by stimulation of D1, and little response found for stimulation of B1, C2, or D1. The latency of the response, 6–8 milliseconds, is consistent with known results (Simons, 1978; Welker et al., 1993); the weak, delayed responses at intervals of ~ 100 milliseconds are typical of somatosensory cortex (Armstrong-James and George, 1988; Schöner et al., 1992). At a location intermediate to the two optical signals (2 in Fig. 12A), stimulation of either C1 or C2 induced a spiking response (Fig. 12C). Finally, with the electrode located at the center of the optical signal for C2 (3 in Fig. 12A), we observed unit activity in response to stimulation of C2 but not other vibrissae (Fig. 12D, and data not shown). Similar results were found with other preparations (n = 3).

The correspondence between the spatial organization of the optical signals and cytochrome *c* oxidase barrels was established for preparations in which extensive trial averaging was used to define the shape of the optical signal. We observed staining patterns in SI cortex similar to those found in past work (Woosley and van der Loos, 1970), as shown in the inset to Figure 13. The alignment between the cortical organization defined by the barrels with that defined by the center of the optical signals is good. The optical signal is largely confined to a single barrel for thresholds > 70%, whereas for relatively low thresholds, e.g., ~ 15% for γ (Fig. 13), there is overlap with nearest and some next-nearest neighbors. Similar results were found with all preparation (n = 4). We conclude from the unit recordings and the cytochrome oxidase-stained barrels that the center of the optical signal for a given vibrissa lies above layer 4 afferents for that vibrissa.

***Spatial organization of the satellite responses in SI.*** The large spatial extent of the optical signal (Figs. 5-7, 11, 13) implies that there is substantial overlap between the responses induced by motion of individual vibrissae. We examined this overlap in detail and consider an example

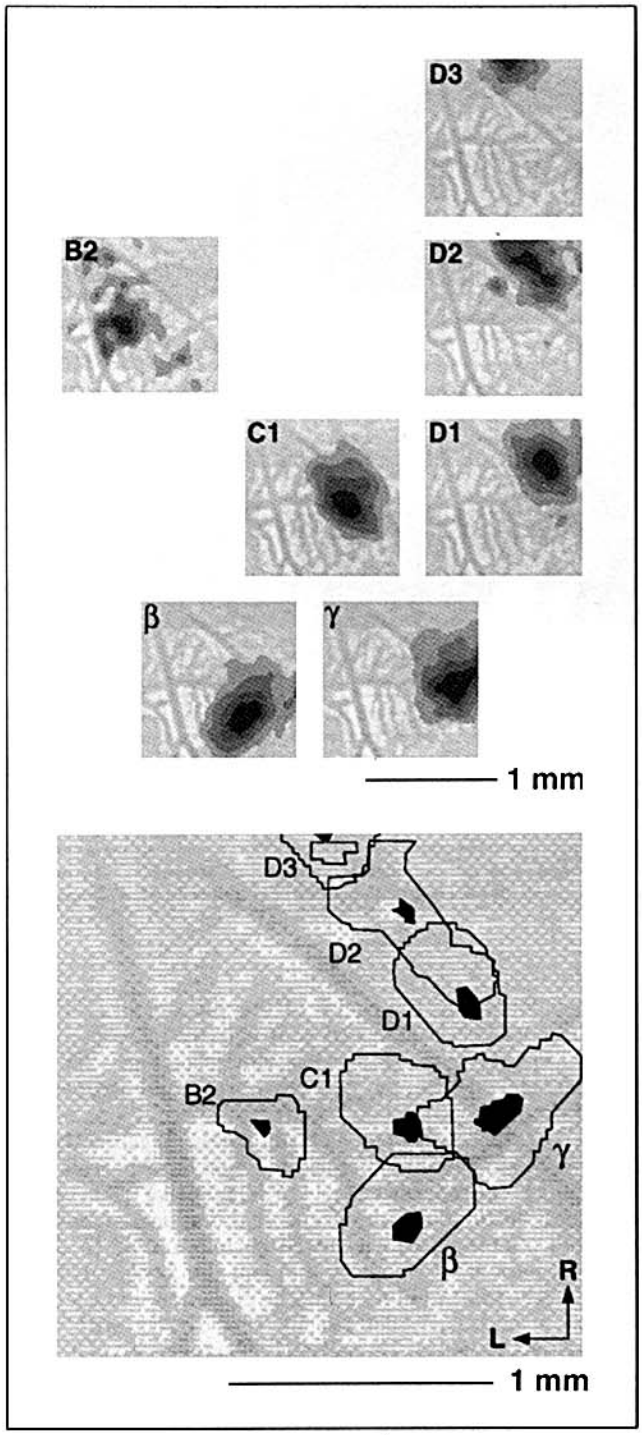


Fig. 11. Map of the major, depolarizing part of the response elicited by motion of different vibrissae. Each vibrissa is stimulated with 25 Hz sinusoids of $\sim \pm 2°$ for five cycles (200 milliseconds). Each response is the average over the first 342 milliseconds (six frames) and 64 trials (21.9 seconds total) and is shown as an overlay on a muted fluorescent image of the cortical blood vessels. The maximal amplitudes of the signals are $-\Delta F/F = 0.00083$ (β), 0.00063 (γ), 0.00053 (B2), 0.00114 (C1), 0.00135 (D1), 0.00055 (D2), and 0.00098 (D3), respectively. The map corresponds to the central region of the optical signal; threshold at 81% of the maximal signal amplitude (Fig. 6). P13 animal.

that involves the individual responses for whiskers C1-C4 (Fig. 14). The satellite region of the signal induced by deflection of C1 was seen to overlap with the central region of C2. Similarly, a satellite region for C4 overlaps with the center for C3. These data show that the satellite region(s) induced by the motion of one vibrissa was aligned with the central region induced by motion of a neighboring vibrissa. The alignment is accurate on the ~100 μm scale of our lateral resolution. A second feature of the data was the alignment of a satellite region of the response for one vibrissa with the central response for next-nearest-neighbor vibrissa (C1 and C3 in Fig. 14). In every experiment in which we measured the response to four or more vibrissae (n = 7 maps), we observed alignment of central and satellite responses for nearest neighbors. Qualitatively, the overlaps were most prevalent in the "row" direction, trivially consistent with elongation of the response in this direction. However, straddlers tended to form triads with their "row" nearest neighbors, e.g., overlap among the responses for γ, C1, and D1 (data not shown). Precise overlaps that involve next-nearest neighbors were seen infrequently (n = 3 maps), not inconsistent with the reduced opportunity for overlaps that span two cortical columns vs. one in our relatively small maps (see, e.g., Figs. 11 and 13).

## Pairwise interactions for single vibrissa activation

The final issue we explored was the optical signal in response to deflection of two vibrissae. Our paradigm was suggested by Simons' (1985) observation that the unit activity elicited by displacing a vibrissa is suppressed if a neighboring vibrissa is previously displaced, a form of forward masking. Each of two neighboring vibrissae was deflected at alternate cycles of a train of sinusoids (inset in Fig. 15). The period of alternation, ~25 milliseconds, was close to that reported to maximize suppression for single consecutive taps (Simons, 1985).[5]

We consider the time-averaged optical signal from an experiment that involves the motion of D1 and D2 (Fig. 15A). Stimulation of each of the two vibrissae resulted in an optical signal whose extent and shape, central region and satellite regions, were similar to those described in the context of individual vibrissa responses (Figs. 5–7, 11, 13). On the other hand, sequential stimulation of the vibrissae as described above led to an optical signal quantitatively different from that predicted from the arithmetic sum of the responses to the individual responses (Fig. 15A,B). The most significant effect was that the maximal amplitude of the optical signal was significantly lower than that of the sum and lower than that of the response induced by stimulation of D1 or D2 alone. This suppression of the optical signal was observed in *all* preparations, by a factor of $1.9 \pm 0.5$ (mean ± SD; n = 11; significant at the $6\sigma$ level). Furthermore, we observed a more variable but, on average, significant increase in the area of the response, by a factor of $1.2 \pm 0.2$ (mean ± SD). Whereas all preparations showed the suppressive effect, only half (5 of 11) showed a significant (at the level of $2\sigma$) increase in spatial extent (cf. Fig.

[5]Our paradigm, which averages the response over a train of displacements, is not equivalent to averaging over trials that involve a single displacement to each vibrissa; in our paradigm, the stimulation appears symmetrical in time after the initial displacement.

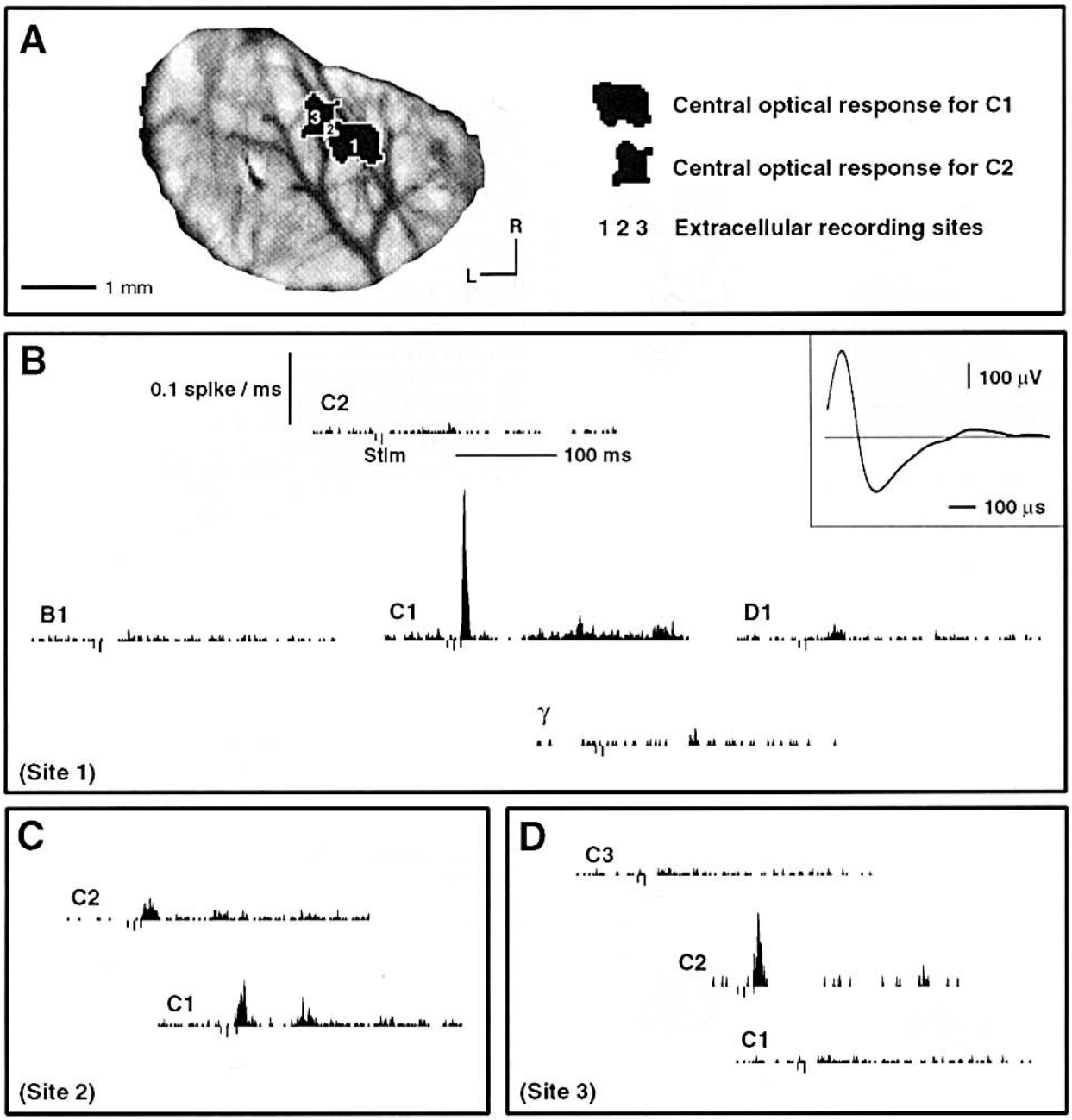


Fig. 12. Relation of the central regions of the optical signal to the unit response, measured with sharp electrodes, at the level of layer 4. Data for a P18 rat anesthetized with 2.0% halothane. **A:** Reference map of the central region of the optical signal induced by stimulation of C1 alone or C2 alone, with each region drawn for a threshold of 60%. The numbers refer to positions of electrode penetrations that are made, to a depth of ~550 mm, upon completion of the optical measurements. Each response is an average over 350 milliseconds (six frames) following the onset of stimulation and 12 trials (4.1 seconds total) with stimulation at 25 Hz and ~ ±2° for 240 milliseconds. Each frame, 100 × 100 pixels, is convoluted with a five-pixel kernel. **B:** Peristimulus histograms (PSTH) of the largest unit (**inset**) at site 1 with respect to stimulation of a given vibrissa with a triangular displacement (rather than the sinusoid). Note that only stimulation of C1 leads to significant activity at site 1; the latency is 7 milliseconds. Each PSTH is the average of 200 trials. The stimulus was a displacement of 3° produced by a step input into an eight-pole Bessel low-pass filter set at 58 Hz. The trigger is shown by the first downward line and the onset of motion, delayed by the filter for ~6 milliseconds, is indicated by the second downward line. **C:** PSTH at site 2. Stimulation of either C1 or C2 leads to spiking at location 2, with latencies of 10 and 7 milliseconds for motion of C1 and C2, respectively. **D:** PSTH at site 3. Only stimulation of C2 leads to spiking at location 3, with a latency of 10 milliseconds. P18 animal.

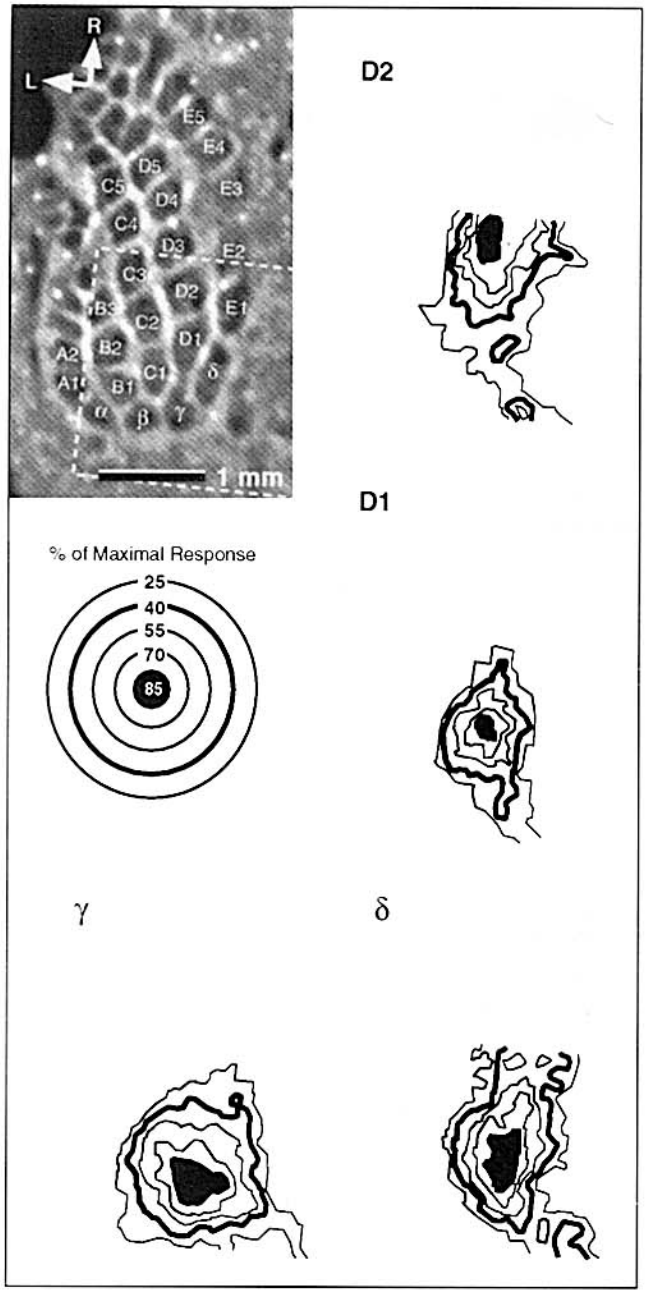


Fig. 13. Relation of the epicenters derived from the optical signal to the distribution of cytochrome oxidase staining at the level of layer 4. We plot the overlap of the optical signal with a drawing of the barrel field derived from a photomicrograph of a section cut parallel to the surface and stained for cytochrome *c* oxidase (**inset**; the image has been digitally filtered). The optical signal is thresholded in increments of 15%, and the contour lines are drawn as seen. Each signal is an average over 560 milliseconds (ten frames) following the onset of stimulation (conditions as in Fig. 10) and 64 trials (36 seconds in total). P15 animal.

15A,B). Finally, on average there was no qualitative difference in the results if the initial order of stimulation was reversed, e.g., D1 → D2 → D1 → . . . vs. D2 → D1 → D2 →. . . . This result suggests that, within the sensitivity of our measurements, the optical signal reflects the steady-state alternation of the two stimuli.

## DISCUSSION

We report on the spatial profile and slow (>50 milliseconds) temporal dynamics of electrical activity as measured with optical techniques. The evidence suggests that our signals originate primarily from the upper part of layers 2/3. First, the cortex is uniformly stained at a depth of 300 μm below the pial surface (Fig. 2), which encompasses layers 2/3, whereas the staining is substantially reduced at the level of layer 4. Second, contributions from layer 1 are minimized by focussing below the cortical surface (Figs. 3, 5B), through the use of anesthetics (Arezzo et al., 1981) and through trial averaging (see below). Third, our signal extends over the length scale of many cortical columns, or barrels (Figs. 13, 14), consistent with the broad responses found in systematic single-unit studies in layers 2/3 and layer 5 (Armstrong-James et al., 1992) and distinct from the narrow responses recorded in layer 4 (Figs. 12, 13).

It is important to recall that dye-related signals are sensitive to changes in the potential across all membranes within the focus depth, ~120 μm (Fig. 3). Thus neurons, whose somata lie outside the band in layers 2/3 that is defined by this depth, but whose dendrites course through layers 2/3, e.g., layer 5 pyramidal cells, may have contributed to our signal. Similarly, glia may have contributed, although the time course of the signal argues against this (Orbach et al., 1984; see below). A second issue is that we integrate the potential over ~50 milliseconds compared to the millisecond time-scale of an action potential. Thus, the dye signal is dominated by subthreshold activity (Grinvald et al., 1982; Kleinfeld et al., 1994), and, in this sense, our results provide information complementary to that obtained from single-unit activity and local-field measurements of extracellular currents.

### Dye vs. intrinsic signals

We have shown that below a minimal level of stimulation the slow, intrinsic optical signal (Fig. 4) was not initiated. This signal reports changes in the scattering properties of cortex (Grinvald et al., 1982; Blasdel and Salama, 1986; MacVicar and Hochman, 1991; Yuste et al., 1996) and changes in the hemodynamics of cortex that are modulated by spiking activity (Grinvald et al., 1986; Frostig et al., 1990). A second issue is that the spatial form of the responses in S1 vibrissae cortex that are determined from intrinsic signals have been reported (Masino et al., 1993; Peterson and Goldreich, 1994) to be punctate compared to the vibrissal evoked dye responses shown here; in fact, they approximate the pattern of cytochrome *c* oxidase staining in the afferent layer (Masino et al., 1993). To the extent that the density of vasculature is greatest at the border of layers 3 and 4 (Patel, 1983), the slow, intrinsic signal may be dominated by hemodynamic changes in or near layer 4.

### Trial averaging

A limitation of the present study was the need for extensive trial averaging (Fig. 5). This did not allow study of trial-to-trial fluctuations in the cortical response and, as a technical issue, severely reduced the number of separate measurements we could perform with a given animal. This limitation originates from noise that is dominated by cardiac pulsations and respiratory motions that are incompletely suppressed by our one-point correction schemes (see Materials and Methods). Two complementary schemes might overcome the need to trial average in the future. The

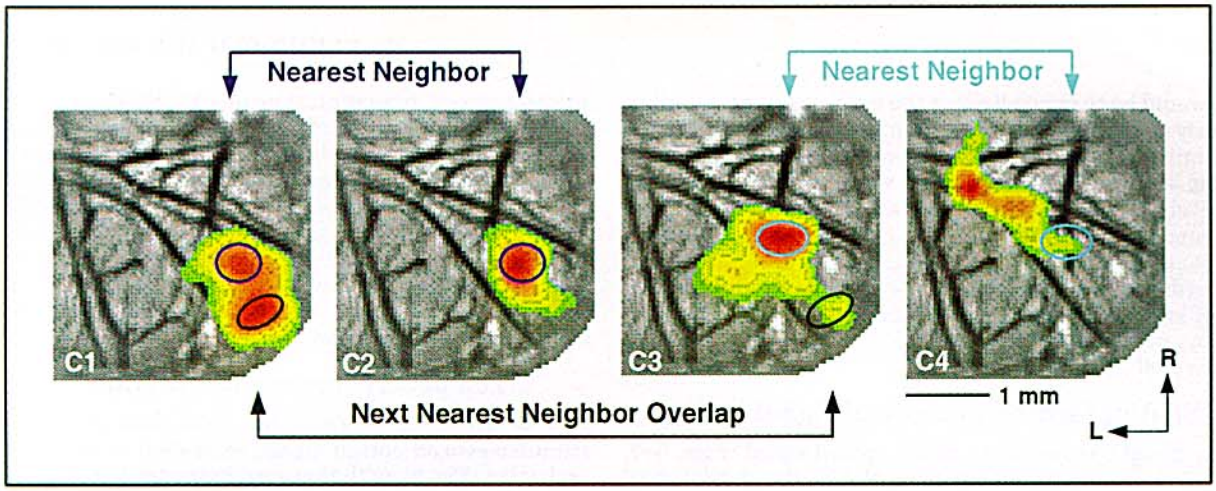


Fig. 14. Overlap of the central regions of the optical signal induced by motion of a single vibrissa with the satellite regions of the optical signal from nearest neighbors and next-nearest neighbors. The optical signals, thresholded at 51% of the maximal value, in response to motion of whiskers C1, C2, C3, and C4. The ovals mark the region of overlap between the central and the satellite regions. We stimulated with 40 Hz sinusoids, ~ ±2°, once every 88 milliseconds (alternate frames). Each response is averaged over 25 milliseconds (eight frames) following the onset of stimulation and 24 trials (6.0 seconds total). P19 female rat.

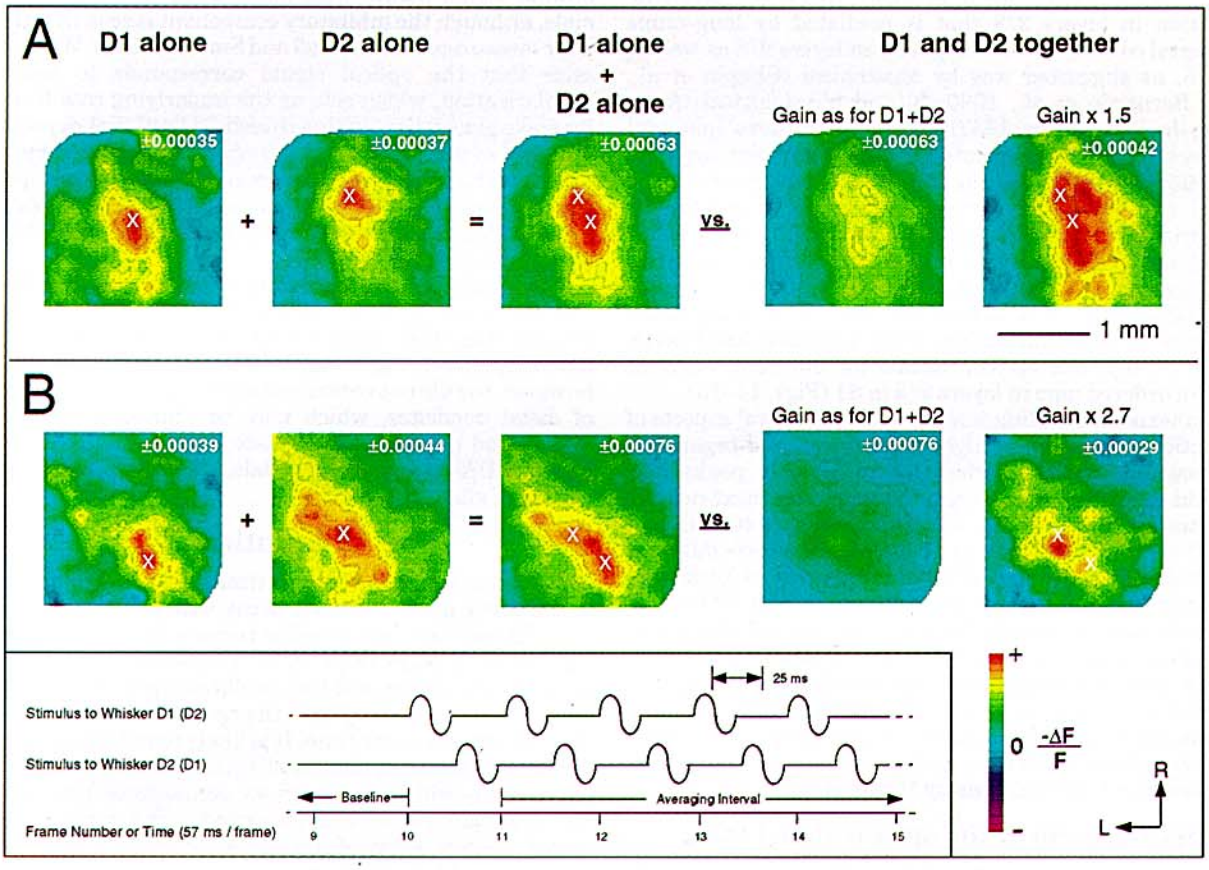


Fig. 15. Suppression of the optical signal by alternate stimulation of two neighboring vibrissae. We recorded the optical signal for each of the two vibrissae stimulated alone and the signal when the vibrissae were stimulated on alternate phases (25 millisecond delay) of a train of stimuli. **A:** The signal is an average over nine frames, or stimuli, and 48 trials (24.6 seconds total), and the color scale is set by the maximal amplitude of the response. The panel marked "D1 alone + D2 alone" is the arithmetic sum of the individual responses. Note that the maximal amplitude of the arithmetic sum is less than that of the individual responses; the maxima for the individual responses occur in different pixels. The panel marked "D1 and D2 together" is the optical signal when both D1 and D2 are costimulated in the order D1 → D2 → D1 → . . . as in A. Note that the maximal amplitude of the signal induced by sequential stimulation is ~1.5 times less than that for the arithmetic sum of the individual responses, and note further that the spatial distribution is different. P17 animal. **B:** Data for a second rat; the paradigm is the same for that shown in A, except that whiskers D1 and D2 were sequentially stimulated in the order D2 → D1 → D2 →. . . . Note the particularly large and elongated response for D2 alone and the high degree of suppression when vibrissae were sequentially stimulated. P20 animal. **Inset:** Schematic representation of the stimulus timing. The stimuli were 17.5 Hz trains (the camera frame rate) of single 40 Hz sinusoids. We averaged the response over the second through the tenth stimuli. Note that, after the onset of stimulation (frame 10), the stimulation of the two vibrissae appears to be symmetric in time. Scaling: All images were printed so that the maximal value of $-\Delta F/F$ corresponded to the maximum of the color scale. The absolute scale factors are given in white in each frame.

first would be to image light at the cortical surface simultaneously at two wavelengths (Kiosita et al., 1991) as a means to eliminate voltage-independent contributions with radiometric techniques. The second would make use of the relatively long correlation time of a train of heart beats. The frequency of the beat, 5–7 Hz, overlaps with frequency components in the depolarizing response (Fig. 9). However, the cardiac contribution is likely to be removed through the use of long data records and estimates (Thomson, 1982) of the magnitude and phase in the cardiac spectral bands (Mitra et al., 1996).

## Spatial form of the optical signal in S1

The broad spatial extent of the optical signal (Figs. 5–7, 11, 13) was not surprising given the electrophysiological data (Armstrong-James et al., 1992) showing divergence of spike activity in a cone-like manner above and below layer 4, the spread of activation seen in deoxyglucose measurements on animals trimmed to have a single vibrissa (McClasland and Woosley 1988), and optical measurements on the spread of activity in primary visual cortex (Grinvald et al., 1994). This spread is likely to reflect dendritic activation in layers 2/3 that is mediated by long-range horizontal collaterals that originate in layers 2/3 as well as layer 5, as suggested was by anatomical (Chapin et al., 1987; Bernardo et al., 1990a,b) and physiological (Armstrong-James and Fox, 1987) studies and by developmental studies of layer 2/3 connectivity (Fox, 1992; Schlaggar et al., 1993). Furthermore, the direction of elongation of the optical signal coincides with the dominant orientation of the horizontal connections (Bernardo et al., 1990a) but is orthogonal to the long axis of the layer 4 afferent barrels (Woolsey and van der Loos, 1970). An analogous role for layer 2/3 and layer 5 collaterals occurs in the primary visual system of rodents (Burkhalter, 1989; Lohmann and Roerig, 1994). Finally, our optical signals for different vibrissae form an ordered map in layers 2/3 in S1 (Figs. 11–13).

An unexpected finding was that the peripheral aspects of the optical signals were highly structured and organized. Displacement of one vibrissa led to satellite peaks that overlaid the central responses of nearest and next-nearest neighboring vibrissae (Fig. 14). This pattern is reminiscent of that seen in visual cortex of mammals, where different hypercolumns are linked by an ordered array of horizontal connections (Lund, 1988; Lohmann and Roerig, 1994). It is our prediction that similarly precise anatomical projections occur in primary vibrissa cortex. An alternate interpretation is that the structured organization of the optical response reflects structure in the afferent input, possibly originating from the ordered, multivibrissae responses recently characterized from unit recordings in ventroposterior medial (VPM) thalamus by Nicolelis et al. (1993).

## Spatial form of the optical signal in S2

The single unit recordings of Carvell and Simons (1986) and related anatomical work by these authors (Carvell and Simons, 1987) show that neurons in S2 respond to very many vibrissae and that there is no organized map of the maximal responses. Here we show, at least on a row-wide basis, that the cortical representations completely overlap (Fig. 10). These data provide indirect support for the notion that neurons in S2 respond best to objects that activate many vibrissae.

There is a caveat associated with our assignment of the relatively weak, lateral response (Fig. 10) to S2. The somatosensory representation in rat (Fabri and Burton, 1991), as in squirrel (Krubitzer et al., 1986), comprises a third somatotopic area, designated parietal ventral (PV). It is possible that the activation lateral to S1 that we report actually occurs in PV, although activation of PV would be expected to lead to a response that is rostral to that seen here (Fig. 10). We find it interesting, independently of this assignment, that the row-by-row response in "S2" is not topographically mapped (Fig. 10), whereas gross somatotopic features are mapped (see, e.g., Krubitzer et al., 1986)

## Temporal sequence of the response

It is useful to contrast the time dependence of the stimulus-evoked optical signal, excitation → inhibition → excitation (Fig. 9), with that seen in the trial-averaged spike train. Chapin et al. (1981) and Armstrong-James and George (1988) measured the stimulus-evoked response in different regions of S1. These authors observed prompt spiking, a period of reduced activity, and a long-lasting period of increased spiking in lightly anesthetized and awake rats (see also C1 response in Fig. 12B); only the prompt signal occurs with more deeply anesthetized animals, although the inhibitory component is seen in intracellular measurements (Carvell and Simons, 1988). We hypothesize that the optical signal corresponds to neuronal depolarization, which acts as the underlying rate function for spike generation, with a threshold level that depends on the level of anesthesia and attention. In partial support of this hypothesis, the time course of the intracellular potential measured from cat primary visual cortex in response to a flashed bar (Volgushev et al., 1993) is quite similar to that of the optical signal (Fig. 9).

The similarity in time scales between the long-lasting depolarization seen optically and that seen in the spike records (Fig. 12B) suggests that this component is dominated by local, regenerative feedback. It is impossible, however, to rule out contributions from slow repolarization of distal dendrites, which may be limited by the ~100 millisecond off rate of glutamate from N-methyl-D-aspartate (NMDA)-type receptors (Dale, 1989), and from depolarization of glia.

## Adaptation

The central region of the optical signal, which lies above the afferent input, does not decay with repetitive stimulation. In contrast, the satellite regions in the periphery of our signal do adapt (Figs. 7, 8). The difference in behavior between the center and the satellites represents a form of adaptation that "sharpens" the spatial distribution of the cortical response over time. It is likely to reflect a difference in the adaptation dynamics of pyramidal-to-pyramidal cell connections within a column vs. connections between columns or columns and septal regions. The upper layers of cortex receive little or no thalamic input (Herkenham, 1980; Lu and Lin, 1993) but rather are driven most directly by spiny stellate-to-pyramidal connections from layer 4 to layers 2/3 (Burkhalter, 1989) or pyramidal-to-pyramidal cell connections from layer 6 to layers 2/3 (Yuste, Tank, and Kleinfeld, unpublished observation). Previous work suggests that the spike rate of thalamocortical afferents targets in layer 4 does not adapt under conditions of continuous stimulation (rat: Simons, 1978; cat: Hellweg et al., 1977). On the other hand, Thomson et al. (1993) reported on paired-pulse measurements of the excitatory postsynaptic potential (EPSP) between monosynaptically

connected pyramidal cells in deep layers of somatosensory cortex and showed that the EPSP adapts, even for relatively long stimulus intervals ( ~ 1 second), when the potential of the postsynaptic target is at rest or hyperpolarized. Conversely, these connections are facilitated when the postsynaptic cell is depolarized.

### Spatially extended inhibition

Alternate deflection of two nearest neighboring vibrissae, with a 25 millisecond lag between vibrissae, always led to a suppression in the expected amplitude of the response (Fig. 15). This finding is consistent with the reduction in instantaneous spike rate that occurs after single, sequential deflections of neighboring vibrissae (Simons, 1985). Analogous effects on spiking are observed at the level of the lateral geniculate nucleus (Nelson, 1991b) and primary visual cortex (Nelson, 1991a) in the cat. A unique feature of the present data is the increased spatial extent of dye signal upon successive deflection of two vibrissae (Fig. 15A). The apparent contradiction between a signal that is lower in amplitude yet typically broader in spatial extent remains to be reconciled.

## CONCLUSIONS

We have reported on the spatial extent and slow dynamics of the electrical activity in primary somatosensory cortex in rat. We suggest that our major findings bring new insight to the architecture and function of primary somatosensory cortex. First, there is a defined spatial pattern of depolarization in S1 in response to the activation of a single vibrissa. This pattern has its largest value above the appropriate barrel and local maxima above the barrels of neighboring vibrissae. We suggest that this pattern reflects a strong functional specificity in the underlying intercolumnar connections. Thus, there may be an optimal sequence of vibrissa contacts during object recognition; a similar conclusion was reached from studies of the timing of spike responses in ventral posterior thalamus (Nicolelis et al., 1993). A second finding from this work is that the spatial extent of the cortical response considerably narrows with repeated stimulation. This is a form of cortical adaptation. We suggest that this might be a means for the rat to accommodate to persistent somatic stimuli and, thus, attain a greater sensitivity to novel stimuli. It will be interesting to test this idea in future experiments through the use of multiple stimuli that are staged seconds apart in time.

## ACKNOWLEDGMENTS

We thank W. Denk for guidance in design of the optical system; M.S. Fee for participating in our initial experiments; B. Friedman for assistance with histological material; A. Gelperin for the use of his laboratory; R.A. Stepnoski for designing the spike-acquisition electronics and the PC-based software to run the CCD camera; D.W. Tank for use of his Macintosh-based CCD software; A. Agmon, D.J. Simons, and R. Yuste for valuable discussions; and F.F. Ebner for encouragement. K.R.D. acknowledges support from the National Sciences and Engineering Research Council of Canada (grant OGPO121698).

## LITERATURE CITED

Arezzo, J.C., H.G. Vaughan, Jr., and A.D. Legatt (1981) Topography and intracranial sources of somatosensory evoked potentials in the monkey. II: Cortical components. EEG Clin. Neurophysiol. *28:*1–18.

Arieli, A., D. Shoham, R. Hildesheim, and A. Grinvald (1995) Coherent spatiotemporal patterns of ongoing activity revealed by real-time optical imaging coupled with single-unit recording in the cat visual cortex. J. Neurophysiol. *73:*2072–2093.

Armstrong-James, M., and K. Fox (1987) Spatio-temporal divergence and convergence in rat SI "barrel" cortex. J. Comp. Neurol. *263:*265–281.

Armstrong-James, M., and M.J. George (1988) Influence of anesthesia on spontaneous activity and receptive field size of single units in rat Sm1 neocortex. Exp. Neurol. *99:*369–387.

Armstrong-James, M., C.A. Callahan, and M.A. Friedman (1991) Thalamocortical processing of vibrissal information in the rat. I. Intracortical origins of surround but not center-receptive fields of layer IV neurons in the rat S1 barrel field cortex. J. Comp. Neurol. *303:*193–210.

Armstrong-James, M., K. Fox, and A. Das-Gupta (1992) Flow of excitation within barrel cortex on striking a single vibrissa. J. Neurophysiol. *68:*1345–1358.

Bernardo, K.L., J.S. McCasland, T.A. Woolsey, and R.N. Strominger (1990a) Local intra- and interlaminar connections in mouse barrel cortex. J. Comp. Neurol. *291:*231–255.

Bernardo, K.L., J.S. McCasland, and T.A. Woolsey (1990b) Local axonal trajectories in mouse barrel cortex. Exp Brain Res *82:*246–253.

Blasdel, G.G., and G. Salama (1986) Voltage-sensitive dyes reveal a modular organization in the monkey striate cortex. Nature *321:*579–585.

Burkhalter, A. (1989) Intrinsic connections of rat primary visual cortex: Laminar organization of axonal projections. J. Comp. Neurol. *279:*171–186.

Carvell, G.E., and D.J. Simons (1986) Somatotopic organization of the second somatosensory area in the cerebral cortex of the mouse. Somat. Res. *3:*213–237.

Carvell, G.E., and D.J. Simons (1987) Thalamic and corticocortical connections of the second somatic sensory area of the mouse. J. Comp. Neurol. *265:*409–427.

Carvell, G.E., and D.J. Simons (1988) Membrane potential changes in rat SmI cortical neurons evoked by controlled stimulation of mystacial vibrissae. Brain Res. *448:*186–191.

Chapin, J.K., and C.-S. Lin (1984) Mapping the body representation in the SI cortex of anesthetized and awake rats. J. Comp. Neurol. *229:*199–213.

Chapin, J.K., B.D. Waterhouse, and D.J. Woodward (1981) Differences in cutaneous sensory response properties of single somatosensory cortical neurons in awake and halothane anesthetized rats. Brain Res. Bull. *6:*63–70.

Chapin, J.K., M. Sadeq, and J.L.U. Guise (1987) Corticocortical connections within the primary somatosensory cortex of the rat. J. Comp. Neurol. *263:*326–346.

Chmielowska, J., M. Kossut, and M. Chmielowski (1986) Single vibrissal cortical column in the mouse labeled with 2-deoxyglucose. Exp. Brain. Res. *63:*607–619.

Dale, N. (1989) The role of NMDA receptors in synaptic integration and the organization of complex neural patterns. In J.C. Watkins and G.L. Collingridge (eds): The NMDA Receptor. New York: Oxford IRL Press, pp. 93–107.

Delaney, K.R., and D. Kleinfeld (1994) Distributed patterns of electrical activity in rat somatosensory cortex in response to whisker deflection. Soc. Neurosci. Abstr. *20:*122.

Diamond, M.E., M. Armstrong-James, M.J. Budway, and F.F. Ebner (1992a) Somatic sensory responses in the rostral sector of the posterior group (POm) and in the ventral posterior medial nucleus (VPM) of the rat thalamus. J. Comp. Neurol. *318:*462–476.

Diamond, M.E., M. Armstrong-James, M.J. Budway, and F.F. Ebner (1992b) Somatic sensory responses in the rostral sector of the posterior group (POm) and in the ventral posterior medial nucleus (VPM) of the rat thalamus: Dependence on the barrel cortical field. J. Comp. Neurol. *319:*66–84.

Fabri, M., and H. Burton (1991) Ipsilateral cortical connections of primary somatic sensory cortex in rats. J. Comp. Neurol. *311:*405–424,

Fox, K. (1992) A critical period for experience-dependent synaptic plasticity in rat barrel cortex. J. Neurosci. *12:*1826–1838.

Frostig, R.D., E.E. Lieke, D.Y. Ts'o, and A. Grinvald (1990) Cortical functional architecture and local coupling between neuronal activity and the microcirculation revealed by in vivo high-resolution optical imaging on intrinsic signals. Proc. Natl. Acad. Sci. USA *87:*6082–6086.

Grinvald, A., A. Manaker, and M. Segal (1982) Visualization of the spread of electrical activity in rat hippocampal slices by voltage sensitive optical probes. J. Physiol. (London) *333:*269–291.

Grinvald, A., E.E. Lieke, R.D. Frostig, C.D. Gilbert, and T.N. Weisel (1986) Functional architecture of cortex revealed by optical imaging of intrinsic signals. Nature *324:*361–364.

Grinvald, A., E.E. Lieke, R.D. Frostig, and R. Hildesheim (1994) Cortical point-spread function and long-range lateral interactions revealed by real-time optical imaging of macaque monkey primary visual cortex. J. Neurosci. *14:*2545–2568.

Hellweg, C., W. Shultz, and O.D. Creutzfeldt (1977) Extracellular and intracellular recordings from cat's cortical whisker projection area: Thalamocortical response transformation. J. Neurophysiol. *40:*463–479.

Herkenham, M. (1980) Laminar organization of thalamic projections to the rat neocortex. Science *207:*532–534.

Kim, H.G., and B.W. Connors (1993) Apical dendrites of the neocortex: Correlation between sodium- and calcium-dependent spiking and pyramidal cell morphology. J. Neurosci. *13:*5301–5311.

Kiosita, K., H. Itoh, S. Ishiwata, K. Hirano, T. Nishizaka, and T. Hayakawa (1991) Dual-view microscopy with a single camera: Real-time imaging of molecular orientations and calcium. J. Cell. Biol. *115:*67–73.

Kleinfeld, D., and K.R. Delaney (1995) The pattern of electrical activity in rat somatosensory cortex reports the direction of whisker deflection. Soc. Neurosci. Abstr., Vol. 21.

Kleinfeld, D., K.R. Delaney, M.S. Fee, J.A. Flores, D.W. Tank, and A. Gelperin (1994) Dynamic of propagating waves in the olfactory network of a terrestrial mollusk: An electrical and optical study. J. Neurophysiol. *72:*1402–1419.

Kossut, M., P.J. Hand, J. Greenberg, and C.L. Hand (1988) Single vibrissal cortical column in S1 cortex of rat and its alterations in neonatal and adult vibrissa-deafferented animals: A quantitative 2DG study. J. Neurophysiol. *60:*829–852.

Krubitzer, L.A., M.A. Sesma, and J.H. Kaas (1986) Microelectrode maps, myeloarchitecture, and cortical connections of three somatotopically organized representations of the body surface in the parietal cortex of squirrels. J. Comp. Neurol. *250:*403–430.

Liu, Y., Q. Gu, and M. Cynader (1993) An improved staining technique for cytochrome c oxidase. J. Neurosci. Methods *49:*181–184.

Lohmann, H., and B. Roerig (1994) Long-range horizontal connections between supragranular pyramidal cells in the extrastriate visual cortex of the rat. J. Comp. Neurol. *344:*543–558.

London, J., L.B. Cohen, and J.-Y. Wu (1989) Optical recordings of the cortical response to whisker stimulation before and after the addition of an epileptogenic agent. J. Neurosci. *9:*2182–2190.

Lu, S.M., and R.-C. Lin (1993) Thalamic afferents of the rat barrel cortex: A light- and electron-microscopic study using *Phaseolus vulgaris* leucoagglutinin as an anterograde tracer. Somatosens. Motor Res. *10:*1–16.

Lund, J.S. (1988) Anatomical organization of macaque monkey striate visual cortex. Annu. Rev. Neurosci. *11:*253–288.

MacVicar, B.A., and D. Hochman (1991) Imaging of synaptically evoked intrinsic optical signals in hippocampal slices. J. Neurosci. *11:*1458–1469.

Masino, S.A., M.C. Kwon, Y. Dory, and R.D. Frostig (1993) Characterization of functional organization with rat barrel cortex using intrinsic signal optical imaging through a thinned skull. Proc. Natl. Acad. Sci. USA *90:*9998–10002.

McCasland, J.S., and T.A. Woolsey (1988) High-resolution 2-deoxyglucose mapping of functional cortical columns in mouse barrel cortex. J. Comp. Neurol. *278:*555–569.

McCormick, D.A., and D.A. Prince (1987) postnatal development of electrophysiological properties of rat cerebral cortical pyramidal neurons. J. Physiol. *393:* 743–762.

Mitra, P. P., B. Pesaran, S. Ogawa, and D. Kleinfeld (1996) Characterization and removal of respiratory, cardiac and vasomotor signals in functional brain images. Soc. Neurosci. Abstr. (in press).

National Institutes of Health (1985) Guide for the Care and Use of Laboratory Animals. NIH Publication 85-23. Bethesda, MD: National Institutes of Health.

Nelson, S.B. (1991a) Temporal interactions in the cat visual system. I. Orientation-selective suppression in the visual cortex. J. Neurosci. *11:*344–356.

Nelson, S.B. (1991b) Temporal interactions in the cat visual system. II. Suppressive and facilatory effects in the lateral geniculate nucleus. J. Neurosci. *11:*357–368.

Nicolelis, M.A.L., C.-S. Lin, and J.K. Chapin (1991) Ontogeny of cortico-cortical connections of the rat somatosensory cortex. Somatosens. Motor Res. *8:*193–200.

Nicolelis, M.A.L., C.-S. Lin, D.J. Woodward, and J.K. Chapin (1993) Dynamic and distributed properties of many-neuron ensembles in the ventralposterior medial thalamus of awake rats. Proc. Natl. Acad. Sci. USA *90:*2212–2216.

Orbach, H.S., and D.C. Van Essen (1993) In vivo tracing of pathways and spatio-temporal activity patterns in rat visual cortex using voltage sensitive dyes. Exp. Brain Res. *94:*371–392.

Orbach, H.S., L.B. Cohen, and A. Grinvald (1984) Optical mapping of electrical activity in rat somatosensory and visual cortex. J. Neurosci. *7:*1886–1895.

Palmer, L.A., and T.L. Davis (1981) Receptive field structure in cat striate cortex. J. Neurophysiol. *46:*260–276.

Patel, U. (1983) Nonrandom distribution of blood vessels on the posterior region of the rat somatosensory cortex. Brain Res. *289:*65–70.

Peterson, B.E., and D. Goldreich (1994) A new approach to optical imaging applied to rat barrel cortex. J. Neurosci. Methods *54:*39–47.

Schlaggar, B.L., K. Fox, and D.D.M. O'Leary (1993) Postsynaptic control of plasticity in developing somatosensory cortex. Nature *364:*623–626.

Schöner G., K. Kopecz, F. Spengler, and H.R. Dinse (1992) Evoked oscillatory cortical responses are dynamically coupled to peripheral stimuli. Neuroreport *3:*579–582.

Simons, D.J. (1978) Response properties of vibrissa units in rat SI somatosensory neocortex J. Neurophysiol. *41:*798–820.

Simons, D.J. (1983) Multi-whisker stimulation and its effects on vibrissal units in rat SmI barrel cortex. Brain Res. *276:*178–182.

Simons, D.J. (1985) Temporal and spatial integration in rat SI vibrissa cortex. J. Neurophysiol. *54:*615–635.

Thomson, A.M., J. Deuchars, and D.C. West (1993) Large, deep layer pyramid-pyramid single axon EPSPs in slices of rat motor cortex display paired pulse and frequency-dependent depression, mediated presynaptically and self-facilitation, mediated postsynaptically. J. Neurophysiol. *70:*2354–2369.

Thomson, D.J. (1982) Spectral estimation and harmonic analysis. Proc. IEEE *70:*1055–1096

Volgushev, M., X. Pei, T.R. Vidyasagar, and O.D. Creutzfeldt (1993) Excitation and inhibition in orientation selectivity of cat visual cortex neurons revealed by whole-cell recordings in vivo. Vis. Neurosci. *10:*1151–1155.

Welker, C. (1971) Microelectrode delineation of fine grain somatotopic organization of SmI cerebral neocortex in albino rat. Brain Res. *26:*259–275.

Welker, E., P.V. Hoogland, and H. van der Loos (1988) Organization of feedback and feedforward projections of the barrel cortex: A PHLA-L study in the mouse. Exp. Brain Res. *73:*411–435.

Welker, E., M. Armstrong-James, H. van der Loos, and R. Kraftsik (1993) The mode of activation of a barrel column: Response properties of single units in the somatosensory cortex of the mouse upon whisker deflection. Eur. J. Neurosci. *5:*691–712.

Welker, W.I. (1964) Analysis of sniffing of the albino rat. Behavior *22:*223–244.

Woolsey, T.A., and H. van der Loos (1970) The structural organization of layer IV in the somatosensory region (S1) of mouse cerebral cortex: The description of a cortical field composed of discrete cytoarchitectural units. Brain Res. *17:*205–242.